

HYDRODYNAMIC EVALUATION OF HIGH-SPEED SEMI-SWATH VESSELS

by

Adam Guttenplan

B.S. Civil Engineering
Columbia University, 2005
B.S. Physics
Hobart College, 2003

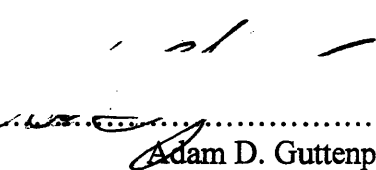
SUBMITTED TO THE DEPARTMENT OF MECHANICAL ENGINEERING IN
PARTIAL FULFILLMENT OF THE REQUIREMENTS FOR THE DEGREE OF

MASTER OF SCIENCE IN NAVAL ARCHITECTURE AND MARINE ENGINEERING
AT THE
MASSACHUSETTS INSTITUTE OF TECHNOLOGY


JUNE 2007

© 2007 Massachusetts Institute of Technology.
All rights reserved


Author:.....

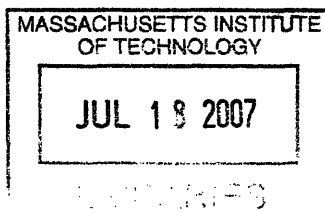

Adam D. Guttenplan
Department of Mechanical Engineering
May 18, 2007

Certified by:.....


Paul D. Sclavounos
Professor of Naval Architecture
Thesis Supervisor

Accepted by:.....


Lallit Anand
Professor of Mechanical Engineering
Chairman, Committee on Graduate Students



ARCHIVES

Hydrodynamic Evaluation of High-Speed Semi-SWATH Vessels

by

Adam Guttenplan

Submitted to the department of Mechanical Engineering on May 18, 2007
in partial fulfillment of the requirements for the degree of
Master of Science in Naval Architecture and Marine Engineering

Abstract

High-speed semi-displacement vessels have enjoyed rapid development and widespread use over the past 25 years. Concurrent with their growth as viable commercial and naval platforms, has been the advancement of three-dimensional computational fluid dynamics codes that simulate steady and unsteady free surface potential flows around ships. The most promising of these computer-based simulations employ a variation of the *Rankine Panel Method*, or R.P.M. R.P.M.'s offer greater prediction accuracy than industry standard two-dimensional strip and slender-body methods, and are enjoying increased use in practical vessel design due to their reliability and low relative cost.

This study uses one such code to examine the high-speed hydrodynamic performance of a slender, semi-SWATH, prototype catamaran with variable demi-hull separation. Hull separation's influence on vessel performance was studied in terms of calm water resistance and seakeeping response in a bare-hull state, and when equipped with quasi-active lifting appendage control. Analysis was performed on a 10.5m, 10,000kg reduced waterplane area catamaran designed by *Lockheed Martin Maritime Systems & Sensors*. In accordance with a non-disclosure agreement, specific hull geometry has been deemed proprietary and is not revealed. Principle vessel dimensions, body, and free surface meshing however, are discussed. The hydrodynamic characteristics of each hull separation and lifting appendage configuration were analyzed by the general purpose, potential flow, time domain, *Rankine Panel Method*, software package, *SWAN2 2002*. An acronym for Ship Wave Analysis, *SWAN2 2002* is a state-of-the-art computational fluid dynamics code developed in MIT in recent years, and is utilized principally as a numerical towing tank.

Thesis Supervisor: Paul D. Sclavounos
Title: Professor of Naval Architecture

Acknowledgments

The following thesis was written and supporting research conducted, during the 2006-2007 academic year in *Laboratory for Ship and Platform Flow* at the *Massachusetts Institute of Technology*, and is the culmination of the author's study at the Institute. The research process has been extremely enlightening and was invaluable in shaping my knowledge as hydrodynamicist, and my graduate student experience as a whole. I would like to express my appreciation to all who supported me through my graduate work making this thesis possible.

I am sincerely grateful to my thesis advisors Professors Paul D. Sclavounos and Capt. Patrick J. Keenan, under whom I studied and assisted in the teaching of several naval architecture and hydrodynamic courses. As a world class hydrodynamicist, Paul's wonderful insight and tireless enthusiasm created an ideal atmosphere under which to perform cutting edge research and increase my understanding of fluid dynamics. To him I say a heartfelt "*ΕΥΧΑΡΙΣΤΩ!*" Capt. Keenan provided expert tutelage in my study of vessel design and worldly career advice from which I continue to benefit in a very real and profound way

I would also like to thank my wonderful parents who diligently encouraged to "Take it one step at a time." and were instrumental in keeping me pointed in the right direction. Their understanding and support during my time here has been invaluable.

Finally, I would like to thank Barbara Smith and the boys of the *LSPF*, particularly my lab mates Nick Parker and Chris Tracy. Their sage-like advice and comedic social commentary made our lab an enjoyable place to study computational fluid dynamics and life in general.

~Adam Guttenplan

Cambridge, Massachusetts May 18th 2007

Table of Contents

Abstract	3
Acknowledgments.....	4
List of Figures	6
Chapter 1: Introduction	8
1.1 Overview.....	10
Chapter 2: Bare Hull Calm Water Resistance.....	11
2.1 Introduction.....	11
2.2 <i>SWAN2</i> Implementation.....	12
2.3 Wave Patterns Predictions.....	14
2.4 Dynamic Sinkage and Trim	18
2.5 Calm Water Resistance	20
2.5.1 Ideal Fluid Resistance	22
2.5.2 Viscous Resistance.....	23
2.5.3 Total Resistance and Verification	25
Chapter 3: Foil Controlled Calm Water Resistance.....	26
3.1 Introduction.....	26
3.2 Hydrofoil Free Surface Interaction	27
3.3 Foil Controlled Calm Water Resistance.....	31
Chapter 4: Bare Hull Seakeeping Response.....	35
4.1 Introduction.....	35
4.2 Heave, Pitch, and Roll Response	36
4.2.1 Head Seas Seakeeping Response	38
4.2.2 Beam Seas Seakeeping Response	41
4.2.3 Port-Bow Seas Seakeeping Response	46
Chapter 5: Foil Controlled Seakeeping Response.....	48
5.1 Introduction.....	48
5.2 Foil Controlled Heave, Pitch, and Roll Response.....	48
5.2.1 Head Seas Seakeeping Response	49

5.2.2 Beam Seas Seakeeping Response	51
5.2.3 Port-Bow Seakeeping Response	52
5.3 Foil Controlled v. Bare Hull Seakeeping Response.....	54
Chapter 6: Discussion and Conclusions.....	58
6.1 Conclusions.....	58
6.2 Recommendations For Future Work.....	60
Chapter 7: References	62
Appendix A: Semi-SWATH Principle Dimensions.....	63
Appendix B: Sway and Yaw Response.....	64
Appendix C: Sample Sinkage & Trim Convergence Log.....	67
Appendix D: Sample Seakeeping Response Log.....	68

List of Figures

Figure 1 <i>Rhino2SWAN</i> Screen Shot	13
Figure 2 Kelvin wake pattern behind a vessel	14
Figure 3 Steady wave patterns for separation ratio of 0.20 at Froude numbers .3 -1.2	15
Figure 4 Steady wave patterns for separation ratio of 0.24 at Froude numbers .3 -1.2	16
Figure 5 Steady wave patterns for separation ratio of 0.30 at Froude numbers .3 -1.2	17
Figure 6 Dynamic sinkage and trim for each separation ratio as a function of Fr.....	19
Figure 7 Hydrodynamic pressure on 0.24 separation at Fr=1.2, Note excessive trim angle	20
Figure 8 Ideal fluid resistance and coefficient as a function of Fr.....	22
Figure 9 Ideal fluid resistance of <i>Molland 4b</i> catamaran, where $2p/L = s/L$	22
Figure 10 <i>Couser's</i> form factor for high-speed catamarans	24
Figure 11 Viscous resistance and coefficient as a function of Fr	24
Figure 12 Total resistance coefficient and resistance as function of Fr.....	25
Figure 13 Lift force required for each separation ratio as a function of Fr.....	27
Figure 14 Fraction of Prandtl lift due to calm free surface as a function of depth Fr <i>Faltinsen</i> (2005).....	28
Figure 15 Required foil angle of attack for each separation ratio as a function of Fr	29

Figure 16 Drag coefficient for each separation ratio as a function of Fr	30
Figure 17 Bare hull & foil controlled hydrodynamic pressure at Froude number 1.2, Note improved trim and pressure distribution exhibited by the foil controlled hull.	31
Figure 18 Ideal fluid resistance coefficient and resistance for bare hull & foil controlled hull	32
Figure 19 Viscous resistance as a function of Fr	33
Figure 20 Total resistance coefficient and resistance for bare hull and foil controlled hull	33
Figure 21 SWAN2 coordinate and motion definition <i>Purvin</i> (2003)	37
Figure 22 Semi-SWATH seakeeping simulation in head seas at 18 knots, Note: Only hull surface below the mean free surface is shown.	38
Figure 23 Heave RAO in head seas for each separation ratio.....	39
Figure 24 Pitch RAO in head seas for each separation ratio	40
Figure 25 Semi-SWATH seakeeping simulation in beam seas at 18 knots.....	41
Figure 26 Heave RAO in beam seas for each separation ratio	42
Figure 27 Pitch RAO in beam seas for each separation ratio	43
Figure 28 Roll RAO in beam seas for each separation ratio.....	45
Figure 29 Semi-SWATH in resonant beam seas where $\lambda / L_{Lwl} = .75$	45
Figure 30 Heave, Pitch, and Roll RAO in $\beta=135^\circ$ seas for each separation ratio.....	47
Figure 31 Foil damped Heave & Pitch response in head seas for each separation ratio.....	49
Figure 32 Conventional high-speed catamaran pitch response in head seas <i>Purvin</i> (2003)	50
Figure 33 Pitch, Heave and Roll RAO in beam seas for each separation ratio.....	51
Figure 34 Heave, Pitch, and Roll RAO in port-bow seas for each separation ratio.....	53
Figure 35 Heave & Pitch RAO of 0.24 separation ratio in head seas.....	54
Figure 36 Heave, Pitch, and Roll RAO of 0.24 separation ratio in beam seas	55
Figure 37 Heave, Pitch, and Roll RAO of 0.24 separation ratio in port-bow seas	57
Figure 38 Review of dynamic trim and total resistance results	59
Figure 39 Avoiding simultaneous pitch and heave response through the use of quasi-active foil control.....	60
Figure 40 Semi-SWATH wetted surface. Note waterplane beam variation fore and aft.....	63

Chapter 1: Introduction

Hydrodynamicists typically define a high-speed vessel as one that regularly operates at Froude numbers in excess of one-half. Although particular hull geometries vary widely from conventional to exotic, such vessels often take the form of slender catamarans. This hull type has become an increasingly popular platform for modern commercial and naval applications. Their increased beam and slender demi-hulls enable the catamaran ferry to carry payloads with greater speed and comfort than possible with a monohull of similar displacement. Equally attractive to modern navies, the high-speed naval catamaran can deliver sailors and a variety of supporting equipment to the fight with unmatched speed and sea-kindliness.

A recent advance in catamaran development has been the advent of SWATH technology, or the Small Waterplane Area Twin Hull. As its name suggests, this vessel is characterized by the small waterplane area of its two demi-hulls. Due to this unique geometry, SWATHs' exhibits a higher natural period in heave and pitch, as well as, lower vertical excitation loads in a seaway *Lewis* (1989). As a consequence, they typically demonstrate superior seakeeping behavior when compared to the traditional catamaran. The SWATH's small waterplane also carries a significant disadvantage, an inherent dynamic instability and susceptibility to resonance in the vertical plane. Therefore, beyond a certain threshold speed, a motion control device must be employed to maintain proper trim regardless of sea state. For this reason, the SWATH is not typically classified as a high-speed vessel.

Independently, the slender catamaran and SWATH technologies are fairly well established. Simple catamarans have been used for hundreds of years by natives of the South Pacific, while the first patent for a SWATH like semi-submerged ship was issued to *CG Lundborg* in 1880. The state-of-the-art in marine vehicle development however, attempts to combine the high-speed performance of the slender catamaran, with the seakeeping attributes of a SWATH, in a single vessel known as a semi-SWATH or reduced waterplane area twin hull. These ships have the geometry of a transom-sterned catamaran abaft of amidships, while forward the waterplane area tapers to that of a SWATH. Precise

geometry of the semi-SWATH evaluated in the present study is withheld in accordance with a non-disclosure agreement, but principle dimensions are available in *Appendix A: Semi-SWATH Principle Dimensions*. A major reason for the delayed development of such a hybrid vessel has been the lack of validated analytical tools capable of predicting their performance in a seaway.

The development of the personal computer over the last two decades has ushered in a new era of powerful analytical naval architecture methods. These tools allow the modern designer to predict hydrodynamic behavior of a proposed vessel electronically, in lieu of costly physical modeling. Although their accuracy in modeling complex flows must still be tank validated, these simulations allow the designer to alter hull geometry and reanalyze performance without time delays associated with rebuilding scale models. Prior to the development of modern computational methods, the hydrodynamics of fluid-body interaction was solved empirically or approximated using so-called two-dimensional strip theory estimations. Strip theory requires the division of the hull wetted surface into a number of long slender strips, enforcing the two-dimensional boundary value problem, and integrating strip solutions along the waterline to arrive at the three-dimensional solution. Accurate results require the vessel to be a “slender body” advancing at relatively slow speeds. Strip theory’s fundamental drawback is its assumption that flow variation in the cross-sectional plane is much greater than variation in the streamwise direction *Faltinsen* (1990). This flow constraint is especially problematic near bulbous bows and transom-sterns, both of which are typical of semi-SWATHs and high-speed craft in general.

A more rigorous approach that leads to greater accuracy requires solving for the full three-dimensional flow around the body at forward speed. One increasingly popular means of solving this problem is through the use of potential flow panel algorithms. Essentially a boundary integral method, the three-dimensional *Rankine Panel Method*, or R.P.M., distributes flow singularities over the body mean wetted surface, creating a potential flow that satisfies Laplace’s Equation throughout the fluid domain. Rankine source and dipole density is determined by the body boundary conditions, free-surface conditions, and the wave radiation condition *Faltinsen* (2005). One such code that uses linear potential flow theory in a R.P.M. scheme to solve for flow around a body has been developed in recent years at *Massachusetts Institute of Technology* by P.D. Sclavounos and

others. Initially a frequency domain code, *SWAN2 2002*, short for Ship Wave ANalysis, is now a fully three-dimensional time domain R.P.M. capable of solving steady and unsteady free-surface potential flow around ships and offshore platforms. Although a linearized free surface is assumed and viscosity neglected, the accurate and efficient wave flow simulations produced by *SWAN2* are ideal for analyzing a variety of advanced marine vehicles. The code's underlying theory is not explicitly covered by this study but the interested reader is directed to *Sclavounos et al (2003)* and the *SWAN2 Theory Manual*.

1.1 Overview

The following study used computational methods for the performance prediction of a prototype 10.5m semi-SWATH designed by *Lockheed Martin Maritime Systems & Sensors*. As is common practice, hydrodynamic ship performance was broken down into calm water resistance and seakeeping response. Vessel resistance was analyzed while advancing at variable forward speed in calm water, and onboard motions were computed in separate simulations containing ambient waves. Due to the anticipated dynamic instability of the semi-SWATH at high speeds, drag and motion response were examined in both a bare-hull and quasi-active foil control configuration. The control system employed was quasi-active in that the angle of attack of lifting appendages was actuated to correct trim instability at speed, and as an ancillary benefit, provided passive heave, pitch, and roll damping. Mounting depth below the mean free surface for the control foils was examined using experimental data and three-dimensional hydrofoil theory. Vessel performance was quantified in terms of calm water drag force, sinkage, trim, and response amplitude operator or RAO in sway, heave, pitch, roll, and yaw motion. Yaw and sway response plots are presented in *Appendix B: Sway and Yaw Response*, but are assumed to be of secondary importance and not explicitly discussed. Three hull separation ratios, i.e. the distance between demi-hull centerlines over the waterline length, were examined to determine hull interaction's impact on resistance and seakeeping behavior. Resistance, sinkage, and trim predictions were performed at forward speeds from 2 to 26 knots, or Froude numbers .1 to 1.3. Seakeeping analysis was conducted at "cruising speeds" ranging from 10 to 20 knots, or Froude regime .5 to 1.0.

Chapter 2: Bare Hull Calm Water Resistance

2.1 Introduction

Calm water resistance, dynamic sinkage, and trim make up the steady state, or time independent, vessel response problem. The time domain, *Rankine Panel Method* code *SWAN2*, was used to determine resistance, sinkage, and trim for three separation ratios, 0.20, 0.24, and 0.30 in a bare hull and quasi-actively controlled state. This chapter presents findings of the bare hull analysis. Foil controlled vessel performance is presented in the Chapters 3 & 5. The 0.20 and 0.30 ratios were chosen to examine the hull interaction design space on either side of the 0.24 ratio chosen by the designer. Calm water performance at forward speeds between 2 to 26 knots was simulated by specifying no ambient waves, and resulting simulations produced time independent forces on each demi-hull. The port-starboard symmetric demi-hulls of the semi-SWATH are terminated by deep transom sterns, at which the hull draft is approximately the maximum keel draft, i.e. little keel rocker is present. As it is the defining characteristic of the semi-SWATH, the vessel studied has a full waterline beam aft that is aggressively tapered forward and terminated by a bulbous bow. The interested reader is directed to *Appendix A: Semi-SWATH Principle Dimensions* for additional information and a waterplane cut rendering.

Differing from cruiser sterns, the transom stern terminates the hull underbody abruptly with a sharp right angle in an effort to create clean flow separation at high speeds. When designed correctly, this separation causes the flow to “see” a longer waterline thereby reducing the relevant Froude number and associated wave making resistance. Clean flow separation however, implies a dry transom subject only to atmospheric pressure. The remainder of the hull is exposed to substantially higher hydrostatic and dynamic pressures. This creates an adverse pressure distribution where integration of body pressure yields a net force impeding the forward motion. For cases where transom sterns

are deep and wide like those of the semi-SWATH, the drag penalty paid for the dry transom can be quite significant.

SWAN2 determines the forces on a vessel advancing at forward speed by direct pressure integration. At any non-zero forward speed in flat water, pressure integration will produce a resultant force in the negative x-direction, which is commonly known as the calm water resistance or drag. By determining resistance through ideal fluid pressure integration, wave making and dry transom induced resistance are combined into a single drag component referred to in this study as the inviscid or ideal fluid resistance. As is the case with all potential flow solvers, *SWAN2* cannot account for fluid viscosity and resulting viscous resistance components acting on the hull. Analytical prediction of viscous effects requires solving the boundary layer problem through the use of computational fluid dynamic RANS codes that are computationally costly and of questionable accuracy. A reasonable approximation of viscous effects can be achieved on the basis of the flat plate friction and a viscous pressure form factor.

2.2 *SWAN2* Implementation

The ideal fluid resistance of any vessel is highly dependent on the shape of its wetted surface and therefore an accurate representation of its three-dimensional form is the first step toward reliable performance prediction. A three-dimensional model of the semi-SWATH was provided by *Lockheed Martin* in the form of an initial graphics exchange specification file, or .IGES file. Although viewable in any three-dimensional CAD program, *SWAN2* cannot accept hull geometries directly from this widely used type file type. Instead it requires a .PLN text file containing the offsets in a specified order and format. More information on the correct formatting procedure is available *SWAN2 User Manual*. To facilitate rapid generation of the required semi-SWATH .PLN file, the *Rhino2SWAN* script was written in MATLAB. Using its GUI interface, the user selects a .IGES source file and the code generates a highly accurate .PLN offset file ready for use in *SWAN2*. A screen shot of *Rhino2SWAN* is provided below.

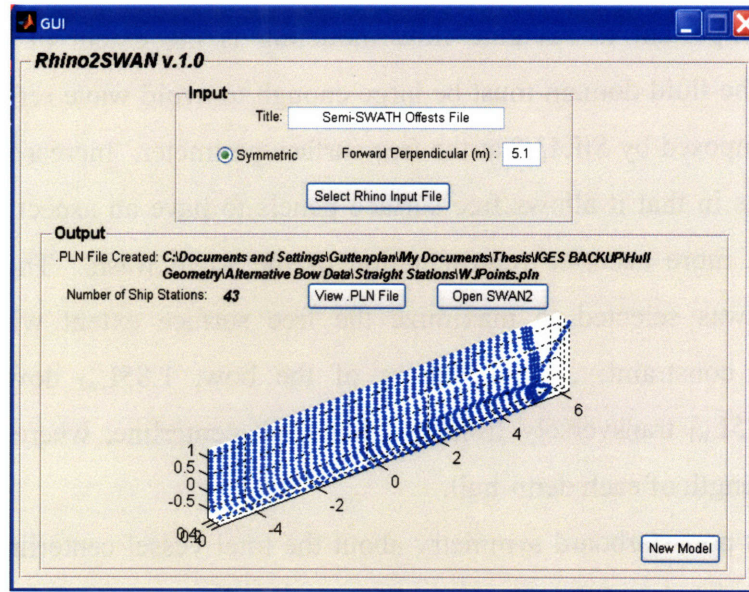


Figure 1 *Rhino2SWAN* Screen Shot

Once created, the .PLN is read by *SWAN2*, which in turn distributes quadrilateral panels over the mean free surface and hull body surface. The mesh density and extents of the free surface discretization must be specified by the user and are crucial to accurate flow modeling. *SWAN2*'s internal meshing routine has an upper limit of 3000 panels to control the computational expense of each simulation. Therefore, the mesh must be chosen such that it is dense enough to accurately represent demi-hull geometry but coarse enough to allow for modeling of a significant portion of the free surface while still using fewer than 3000 panels. Selecting mesh extent and panel size is further complicated by the fact that free surface and body panels share the same dimension in the streamwise direction. In addition, body panel size is not input directly but is instead specified by the number of panels along the hull's waterline length and beam.

Sensitivity checks were performed at low forward speed with various panel combinations to ensure *SWAN2*'s hull form was consistent with known hydrostatic parameters. A visual inspection of the body surface was also performed in *SWAN2*'s companion program *TECPLOT*. The combination of 22 panels in the streamwise direction and 12 in the transverse produced an adequate representation of the hull surface while still leaving a significant number of panels for use in free surface discretization. This grid was kept constant and only altered slightly for problematic Froude numbers.

Equally important to accurate flow modeling is the extent of the free surface discretization. The fluid domain must be large enough to avoid wave reflections from the artificial beach imposed by *SWAN2* at the free surface perimeter. Increased domain size is also advantageous in that it allows free surface panels to have an aspect ratio of roughly one promoting a more accurate representation of the wake wash. The following free surface domain was selected to maximize the free surface extent without exceeding maximum panel constraint: $.5L_{wl}$ upstream of the bow, $1.85L_{wl}$ downstream of the transom, and $1.25L_{wl}$ transversely from the demi-hull centerline, where L_{wl} is the zero speed waterline length of each demi-hull.

Due to its port-starboard symmetry about the total vessel centerline, only the port demi-hull was modeled in *SWAN2*. In addition to the free surface described above, the fluid between the demi-hulls was also modeled to centerline of the complete vessel. The width of this surface was dictated by the hull separation ratio and it was this parameter that was varied to examine demi-hull interaction and its effect on calm water performance.

2.3 Wave Patterns Predictions

Essential to prediction of the calm water resistance, semi-SWATH steady state wave patterns were found for each separation ratio at Froude numbers .1 to 1.3. All the wave patterns conform to a *Kelvin Wake Pattern* with the wave train lying within the 35.16° envelope shown in the figure at right.

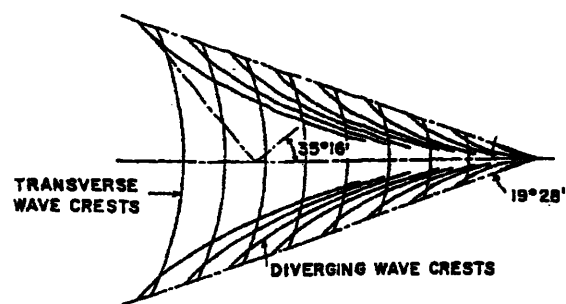


Figure 2 Kelvin wake pattern behind a vessel

The following snapshots show the steady wave pattern behind the semi-SWATH with separation ratios of 0.20, 0.24, and 0.30 advancing at forward speeds corresponding to Froude numbers 0.3 to 1.2. The scale at the top of each figure indicates wave elevation above the mean free surface where blue representing a wave trough, red a crest, and green a zero wave elevation. Only the port demi-hull is shown but the presence of the other hull is accounted by a numerical wall commonly referred to in potential flows as the *methods of images*.

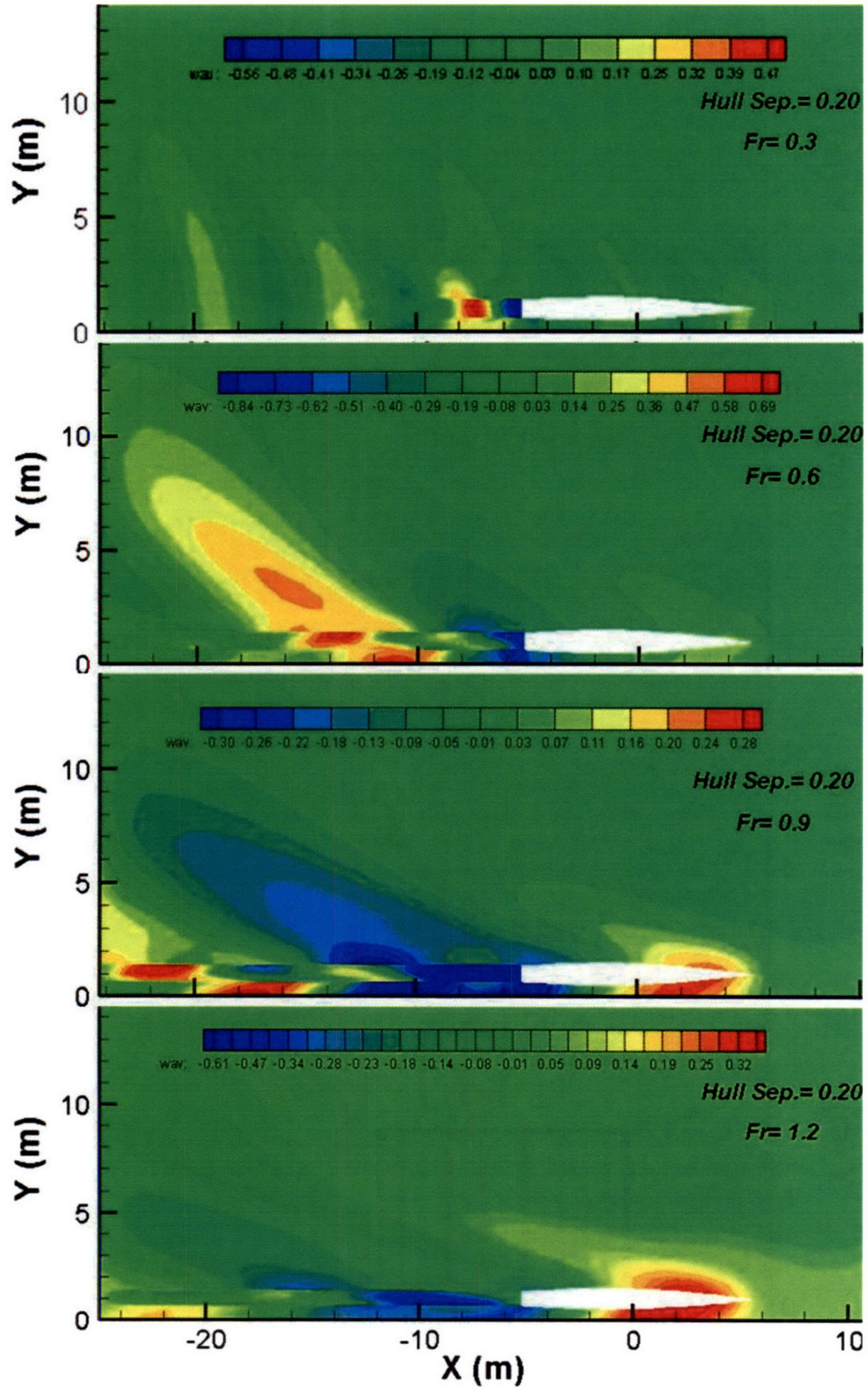


Figure 3 Steady wave patterns for separation ratio of 0.20 at Froude numbers .3 -1.2

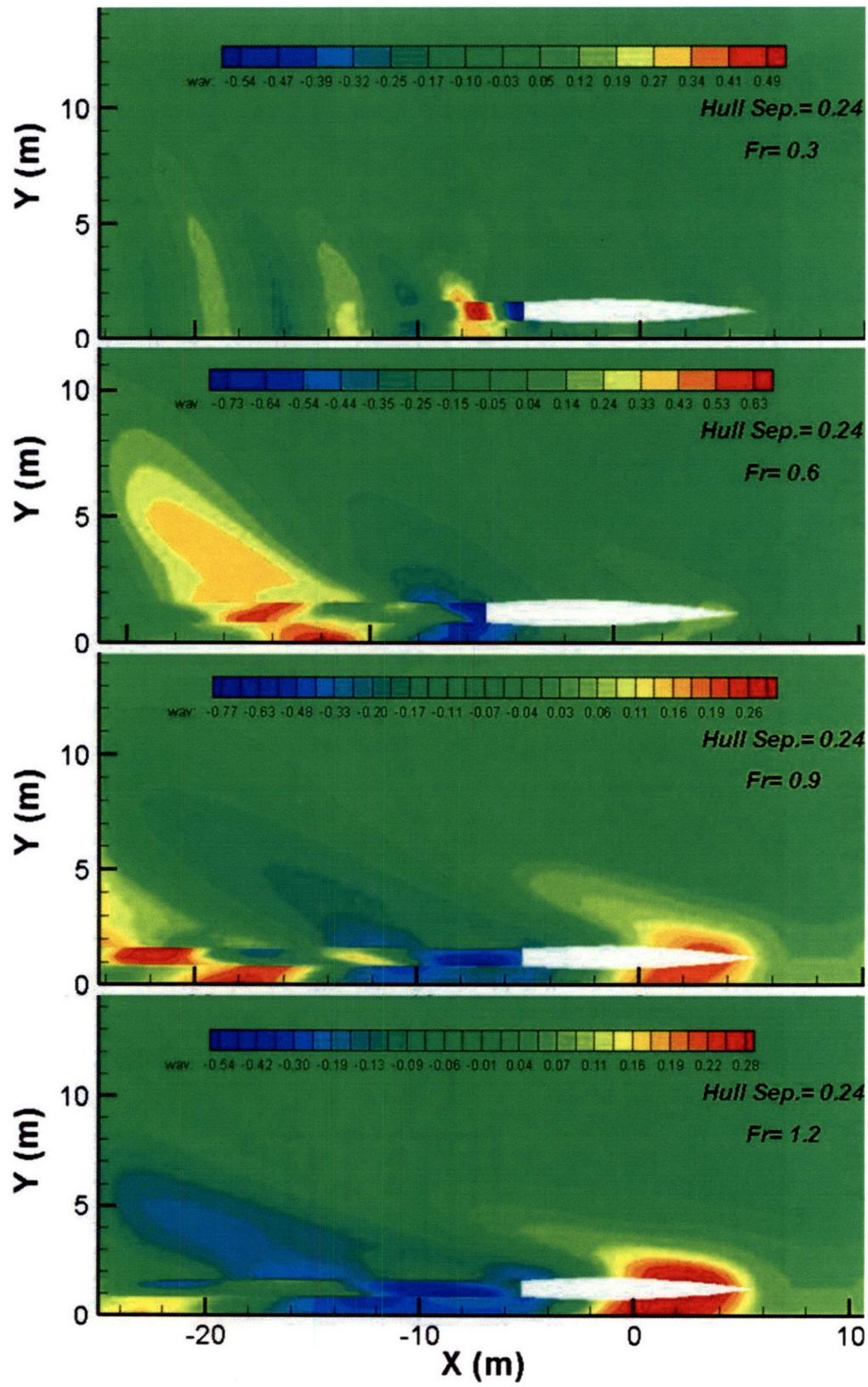


Figure 4 Steady wave patterns for separation ratio of 0.24 at Froude numbers .3 -1.2

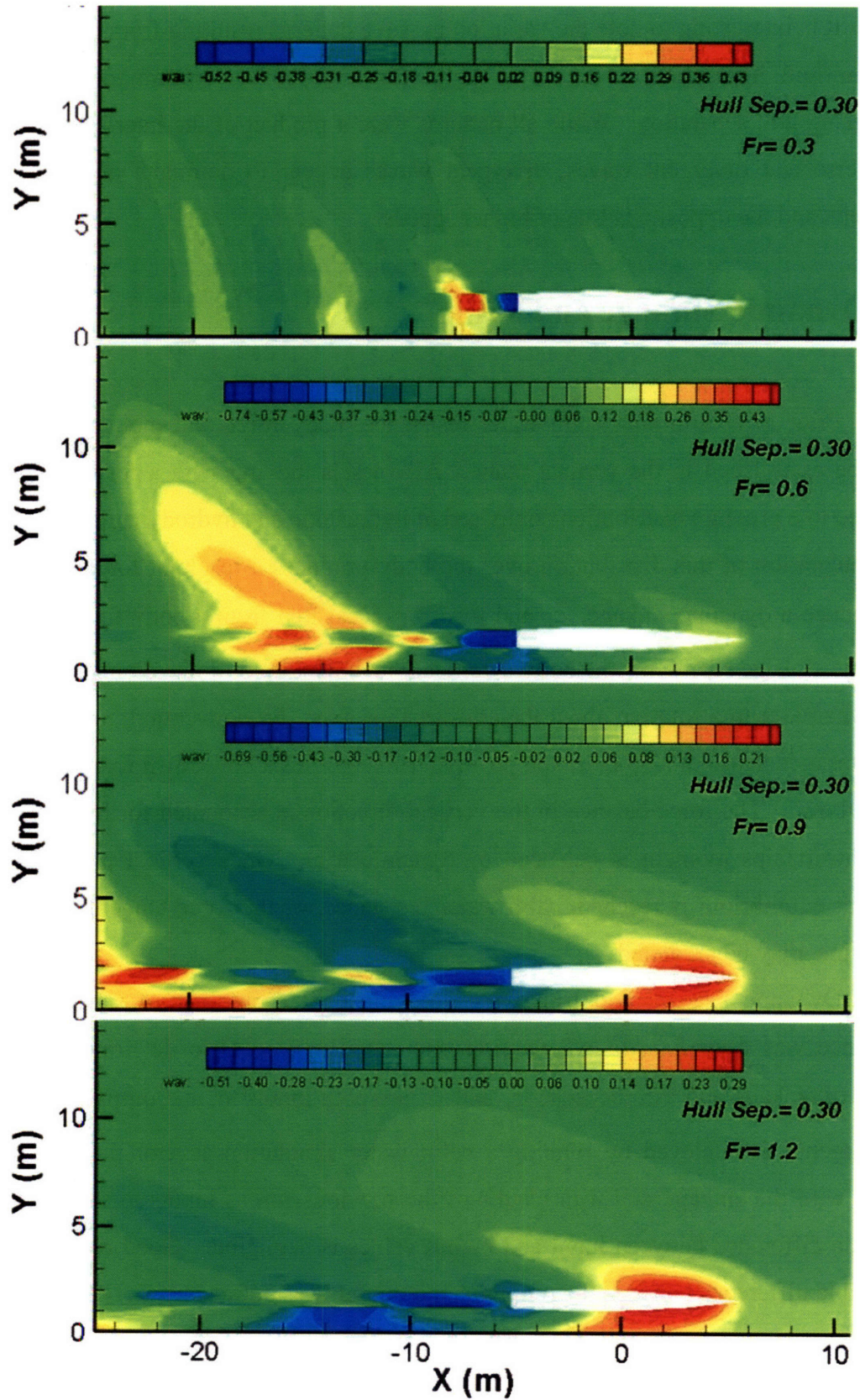


Figure 5 Steady wave patterns for separation ratio of 0.30 at Froude numbers .3 -1.2

It is interesting to note the variation in wave patterns resulting from different levels of demi-hull interaction. Not surprisingly, the interference appears to increase with decreasing hull separation. While all patterns were a product of the interference between transverse and divergent waves, divergent waves appear to dominate at lower Froude numbers, and the opposite is true of higher speeds.

2.4 Dynamic Sinkage and Trim

Prior to determining calm water resistance, body force and moment equilibrium must be established in the vertical plane. All vessels moving with a forward speed are exposed to a pressure distribution composed of hydrostatic and hydrodynamic components. The integration of this distribution over the body produces a resultant force and moment that induce a dynamic sinkage, ζ_3 and trim, ζ_5 . Measured from a body fixed coordinate, dynamic sinkage represents the body's vertical movement up or down along a vertical axis and dynamic trim a rotation about the athwartships axis. By convention, positive sinkage indicates a decrease in ship draft and positive trim signifies a bow down rotation or a "trim by the bow". The force balance in the vertical direction is accounted for by sinkage, and the athwartships moment is balanced by dynamic trim. Once vertical plane force and moment equilibrium is reached, calm water resistance, or the force tangent to the vessel centerline, may be predicted.

Dynamic sinkage and trim were determined at each forward speed for which resistance was desired. *SWAN2* requires an iterative process to determine convergent values of sinkage and trim because ζ_3 and ζ_5 are both inputs to, and outputs of the code. Convergence is achieved by running a calm water simulation several times at a given speed, with the sinkage and trim results of the previous run as inputs to the current run, until the difference between input and output values is negligible. Good convergence, or negligible difference between the run input and output, was defined by (2.1) and (2.2).

$$(2.1) \quad \textit{Sinkage}: |\zeta_{3_n} - \zeta_{3_{n-1}}| \leq .001m \qquad (2.2) \quad \textit{Trim}: |\zeta_{5_n} - \zeta_{5_{n-1}}| \leq .005^\circ$$

SWAN2 was executed within a MATLAB script that performed simulations until convergence was satisfied for each separation and forward speed. Typically, 12 runs or

less were needed to satisfy expressions (2.1) and (2.2). See *Appendix C: Sample Sinkage & Trim Convergence Log* for a sample sinkage and trim code output. The resulting converged dynamic sinkage and trim for each separation ratio is presented in the following figure. Semi-SWATH results are plotted along with ζ_3 and ζ_5 of a conventional high-speed catamaran studied by *Molland et al (1996)*, dimensionalized for agreement with semi-SWATH draft. Demi-hull separation ratio is denoted by s/L in all subsequent plots of this study.

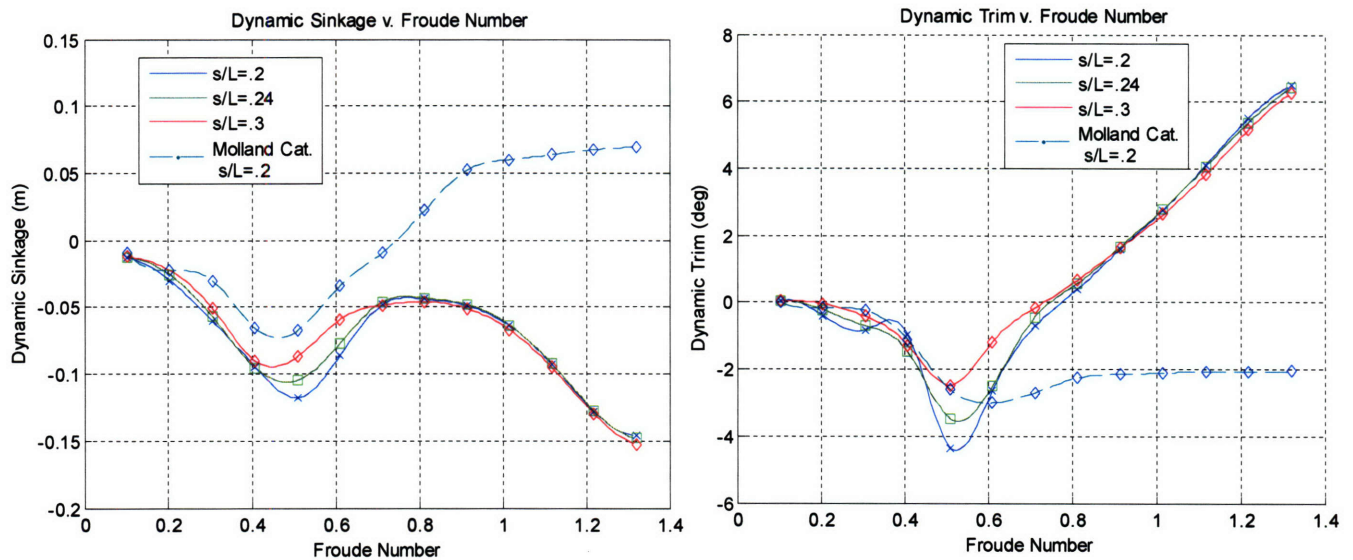


Figure 6 Dynamic sinkage and trim for each separation ratio as a function of Fr

The general trend of increasing negative sinkage with speed was consistent over all separation ratios and indicates a net loss in pressure over the still water hydrostatic pressure. The small decrease in sinkage between Froude numbers .5 and .75 may represent dynamic pre-planning lift induced by the trim by the stern shown in the adjacent trim plot. The semi-SWATH exhibited similar behavior to the conventional *Molland 4b* catamaran at speeds up to Froude number.75. Beyond this threshold, the semi-SWATH's reduced forward waterplane required increasing sinkage to balance hydrodynamic suction. It is interesting to note the relationship between sinkage and hull separation ratio around Froude number .5, where narrower separations produced the more sinkage. Adverse potential flow interactions between the narrowly spaced demi-hulls may account of increased sinkage with decreased s/L .

Examination of the dynamic trim results indicated a rising bow response at lower speeds and bow plunging tendency at higher ones. Once again, low speed behavior is consistent with established high-speed catamaran behavior demonstrated by *Molland*. However, an abrupt break with conventional vessel response occurred at Froude number .75. Above this threshold, a steady bow down trim increased linearly with Froude number. At high speeds, excessive bow diving was observed and is a clear indication of the dynamic instability in the vertical plane. The hydrodynamic pressure on the 0.24 separation at Froude number 1.2 is shown in the figure below.

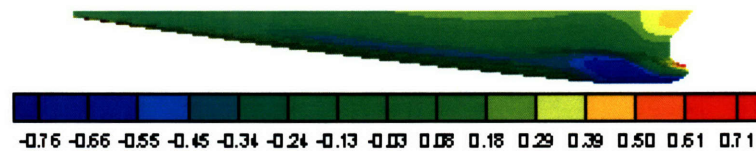


Figure 7 Hydrodynamic pressure on 0.24 separation at Fr=1.2, Note excessive trim angle

The proximity of the red stagnation point to the blue low pressure area indicates a large pressure gradient that imparting a *Munk Moment*, or net downward force, to the bow. With its small waterplane area forward, the semi-SWATH must trim bow down well below the design waterline to generate sufficient hydrostatic righting moment needed to maintain equilibrium. Noting that the transom draft in Figure 7 is nearly zero, it may be assumed the bare hull trim angles are outside the realm of practicality. Accordingly, a quasi-active foil system was designed to correct dynamic trim and is employed subsequent chapters.

2.5 Calm Water Resistance

The resistance of a ship advancing with a forward speed U , is defined as the force required to tow such a vessel at U provided the presence of the tow vessel does not impact the flow around the ship. This force is typically measured in a simplified case in which the ship has no external appendages, where the resulting force is known as the total bare hull resistance. Resistance is often transformed into a non-dimensional coefficient for ease of comparison to other vessels. The expression below is the standard definition of the resistance coefficient where D is the drag force to be non-dimensionalized, ρ is the fluid density, S is the wetted hull surface area.

$$(2.3) \quad C_D = \frac{D}{\frac{1}{2} \cdot \rho \cdot S \cdot U^2}$$

The calm water bare hull resistance of a ship, neglecting air resistance, is due to shear and normal fluid stresses acting on the vessel's wetted surface. The shear stress is wholly due to the viscous nature of the water, while the normal stress component is slightly more complex and may be separated into two major groups. The first of which is wave making resistance, or the component responsible for the generation of inviscid free surface gravity waves. Viscous pressure drag represents the other component and is caused by the pressure deficit at the stern due to the presence of the boundary layer *Cousser* (1997). The actual normal pressure acting on the underbody run and transom is lower than is predicted by potential flow and gives rise to a drag force often called form resistance. As discussed earlier, high-speed vessels employing a transom stern have an additional induced resistance component due to their dry transoms and demi-hull interaction.

SWAN2's integration of normal pressure on the body is especially well suited to predicting wave making, transom induced, and interaction induced drag. These components are often grouped together and are commonly known as the ideal fluid resistance. As an inviscid computational fluid dynamics tool, *SWAN2* cannot predict tangential stresses or normal stresses arising from fluid viscosity. This is unfortunate for analysis of catamarans or semi-SWATHs operating at Froude numbers greater than .6. Above this speed, total resistance is dominated by its viscous component. This effect is so pronounced in .6-1.0 range, the viscous resistance component is on average 4 times greater than the ideal fluid resistance. This fact is particularly regrettable for present study because viscous effects are predicted on the basis of flat plate friction and an empirical form factor.

Calm water resistance of the semi-SWATH was evaluated at speeds of 2 to 26 using the converged sinkage and trim for each speed. As is consistent with hydrodynamic practice, drag force and coefficients are presented as a function of *Froude Number*, the non-dimensional quantity defined by the vessel speed, over the root of waterline length times gravitational acceleration. The waterline length of the vessel the semi-SWATH is approximately 10.5m therefore the speed range tested corresponded to $Fr = .1 - 1.3$.

2.5.1 Ideal Fluid Resistance

The following figure presents the ideal fluid resistance and coefficient.

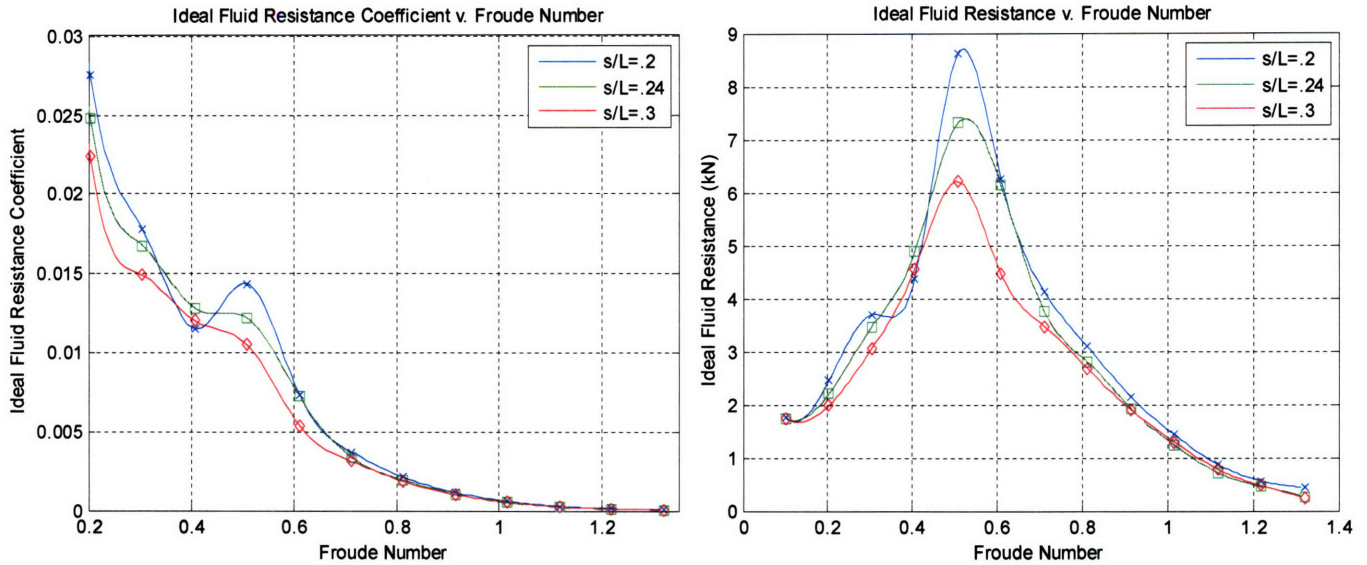


Figure 8 Ideal fluid resistance and coefficient as a function of Fr

As is evident in the figure above, demi-hull separation had an appreciable effect on semi-SWATH ideal fluid resistance. This was especially true near $Fr=0.55$, the so called “Froude Hump” for a displacement vessels. At this speed, narrower separations paid a clear drag penalty over larger ones. At ± 0.15 of the hump, adverse potential flow interactions between closely spaced demi-hulls produced larger resistance coefficients and hence resistances than wider spaced designs. Outside this range, hull separation had a waning influence on resistance. The fluid ideal resistance for the *Molland 4b* catamaran is shown below and is presented to validate general trend of increasing resistance with decreasing hull separation ratio.

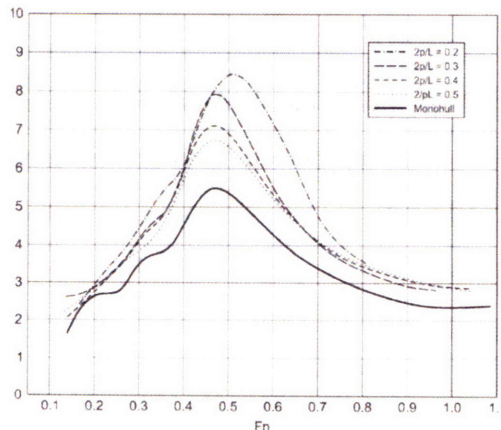


Figure 9 Ideal fluid resistance of *Molland 4b* catamaran, where $2p/L = s/L$

2.5.2 Viscous Resistance

Although only an approximation, flat plate friction has gained wide acceptance in the prediction of vessel frictional drag and was used in this study. The ITTC 1957 line presented in equation (2.7) is valid for viscous drag over a flat plate by predicting tangential stress imparted to a flat plate based on Reynolds number. Normal stress induced by the presence of the boundary layer, or form drag, is accounted for by means of a form factor, k . This empirical factor describes the three dimensional nature of the ship hull and its effect on boundary layer growth associated viscous pressure drag. The form factor is essentially a ratio of the total viscous drag to the flat plate friction as shown by expression (2.4).

$$(2.4) \quad 1 + k = \frac{C_{Viscous}^{actual}}{C_{Friction}^{flat_plate}}$$

An empirical method derived from model testing of high-speed catamarans has been suggested by *Steen* (1999) to determine k . *Steen* asserts that k is a function of length to displacement ratio, when those ratios are between 6 and 12. Although the length to displacement ratio of the semi-SWATH examined is slightly below 6, this method remains the most straightforward means of estimating viscous pressure drag and therefore was used throughout this study. The form factor was determined by the expression below.

$$(2.5) \quad 1 + k = 3.4275 \cdot \left(\frac{L_{wl}}{\nabla^{1/3}} \right)^{-0.443} \quad (2.6) \quad \frac{L_{wl}}{\nabla^{1/3}}$$

By convention, length to displacement ratio is a non-dimensional coefficient given by expression (2.6), $\frac{L_{wl}}{\nabla^{1/3}} = \frac{10.5m}{(5.74m^3)^{1/3}} = 5.86$, and the resulting form factor is given by

expression (2.7), $1 + k = 3.4275 \cdot 5.86^{-0.443} = 1.57$. This result was verified by suggested form factors for high-speed, round-bilge catamarans, presented by *Couser* (1997). Form factors were listed in tabular form for length to displacement ratios of 6.3 to 9.5. These results were extrapolated with a cubic spline to determine the form factor corresponding to the 5.86 ratio of the semi-SWATH. The figure below shows the spline extrapolation of *Couser's* data and confirms the accuracy of result obtained by (2.5).

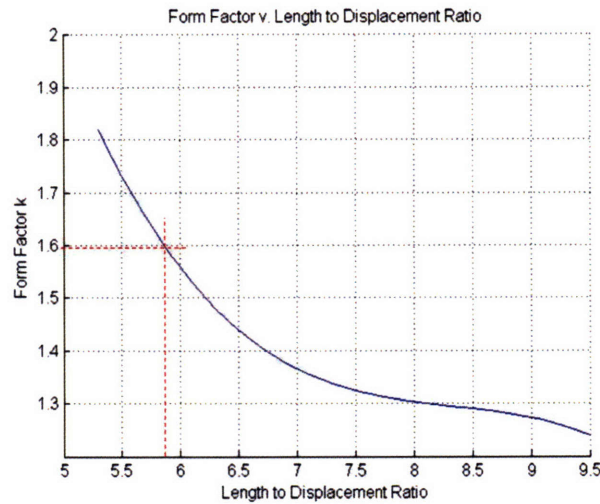


Figure 10 Couser's form factor for high-speed catamarans

As previously mentioned, resistance due to tangential stress on the hull was approximated by the flat plate friction. The flat plate friction based on Reynolds number, (2.6) and wetted surface area from *SWAN2*, was given by the ITTC 1957 line best fit expression (2.7).

$$(2.6) R_n = \frac{U \cdot L}{\nu}$$

$$(2.7) C_f = \frac{0.075}{(\log_{10} R_n - 2)^2}$$

The total viscous drag coefficient was computed using formula (2.4) and was presumed constant for all separation ratios. Form factors are independent of demi-hull separation, as is wetted surface area, and therefore this is a valid assumption.

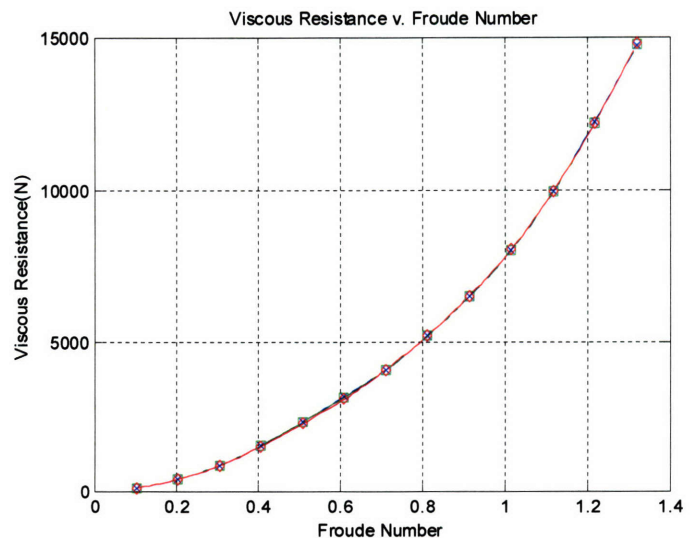
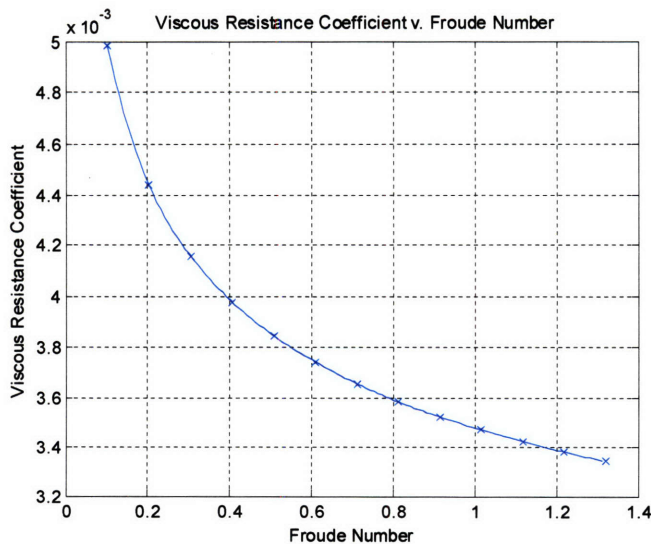


Figure 11 Viscous resistance and coefficient as a function of Fr

2.5.3 Total Resistance and Verification

Total vessel resistance was obtained by summing the ideal resistance obtained from *SWAN2* and the empirically approximated viscous resistance. It should be noted the analysis above neglects aerodynamic, eddy, and spray making resistance. The slender underbody and streamlined superstructure of the semi-SWATH suggest these components will offer only a minor increase in total resistance. The following figure presents the total resistance coefficient as well as the dimensionalized total drag.

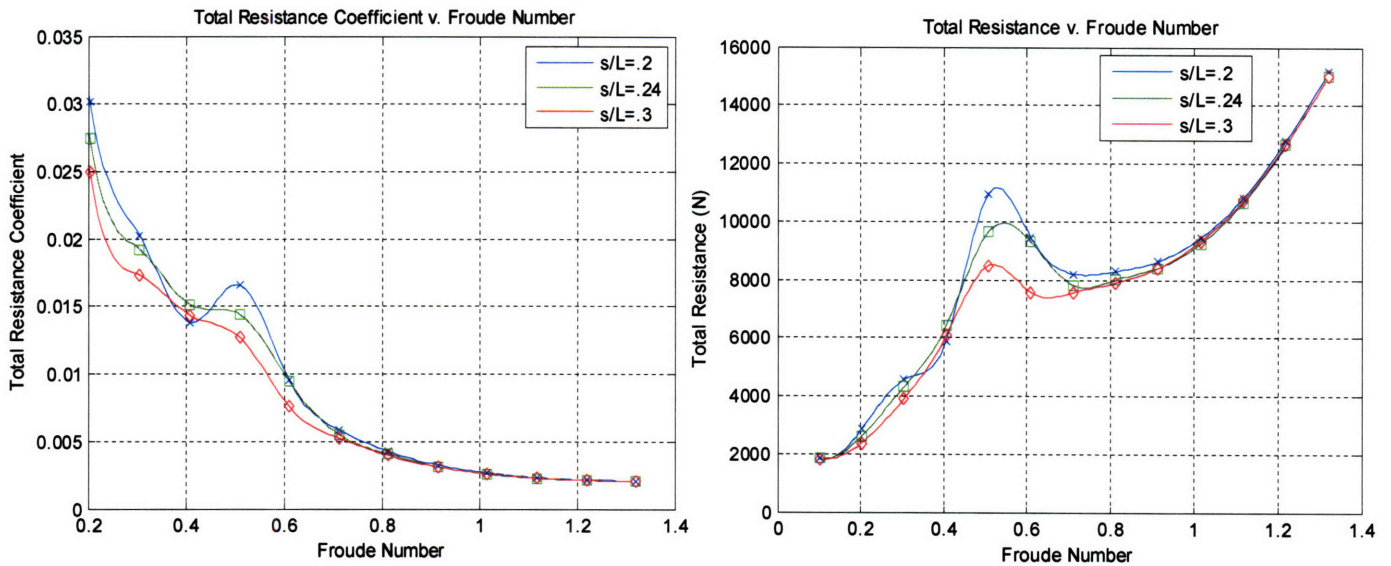


Figure 12 Total resistance coefficient and resistance as function of Fr

As stated above, there was an appreciable difference in the drag force experienced by each separation ratio near speeds corresponding to Froude number .55. At this speed, the 0.30 separation ratio exhibits better, and the 0.20 ratio poorer performance, than the “as designed” 0.24 spacing. This effect was confirmed by the *Molland 4b* data and may be attributed to detrimental flow interactions between the demi-hulls. Elsewhere in the speed range, hull separation appears to have little impact on resistance. Although a simple increase in hull separation improved performance from a resistance and trim standpoint, wave induced structural loads increase with the square of this distance and so hydrodynamic benefits must be tempered against the need for increased structural support.

Chapter 3: Foil Controlled Calm Water Resistance

3.1 Introduction

The calm water bare hull results presented in Chapter 2 showed the semi-SWATH to have significant dynamic instability in the vertical plane. Forward speeds above Froude number .7 generated a large destabilizing *Munk Moment* that resulted in bow diving and a steady trim by the bow. This response is a direct result of the bow pressure distribution as seen in Figure 7. As previously stated, the vessel's fine bow entry and a small waterplane forward require a significant trim by the bow to maintain moment equilibrium during high-speed operation. Hydrodynamicists have recognized this problem in similar craft and have suggested the use of lifting appendages to provide trim stabilization. By applying an upward force near the bow or a downward force near the stern, proper trim can be maintained throughout the speed range. Ensuring operation at or near the design trim, i.e. zero speed trim, is thought to provide both resistance and seakeeping benefits.

Generating the vertical force necessary to maintain a desired trim angle requires modifying inflow velocity, and consequently pressure distribution, around a moving ship. Pressure distribution is a function of forward speed and therefore requires appendage response to vary with speed. Flow around similar vessels is altered through the use of trim tabs, interceptors, canards, and fixed or retractable T-foils. Canards, or horizontal lifting fins, were chosen for control of the semi-SWATH in this study. A forward mounting position was selected because *Sclavounos et al* (2003) argues optimal heave and pitch reduction is obtained by placing surfaces as far forward as practical. For the purposes of the present analysis, a quasi-active system varied canard angle of attack in unison based strictly on controlling calm water forward speed trim. More sophisticated feedback systems exist for controlling dynamic motions in a seaway but are beyond the scope of this

study. Calm water ideal fluid resistance was predicted for each separation ratio at design trim maintained by the quasi-active bow foils.

Finally, foil mounting depth below the free surface was examined. Given the shallow forward draft of the vessel .75m, canard free surface interaction could not be neglected. Appendage depth beneath the free surface was varied and the corresponding lift loss due the free surface was treated with experimental data available in *Faltinsen (2005)*.

3.2 Hydrofoil Free Surface Interaction

A *SWAN2* simulation was performed for each hull separation ratio in the 2 to 26 knots speed range. Simulations were run in calm water with the body held fixed in all modes of motion at the design waterline. The dynamic trimming moment was extracted from *SWAN2* output and used to determine the precise moment needed to maintain zero trim at each speed step. The quasi-active system imparts a moment equal in magnitude but opposite in sign to the trimming moment by two bow-mounted, symmetric, uncambered foils. Each foil has moderate an aspect ratio of $\Lambda = 1.6$, and an elliptical planform area of $.5\text{m}^2$, or 1.2% of the total wetted hull surface area. Each canard was fixed 5m forward of amidships and by dividing the trim moment by this lever arm, the force required from each foil was determined and is given in the figure below.

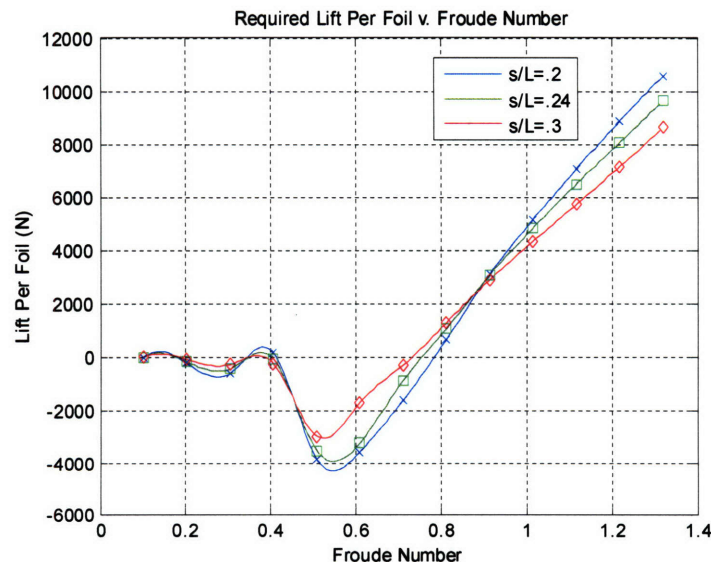


Figure 13 Lift force required for each separation ratio as a function of Fr

Given the lift force needed at each speed, a lift coefficient, C_{Lreq} , was derived from an analogous expression to the drag coefficient given in (2.3), in which S is the foil planform area. A foil operating near the free surface however, will rarely achieve its infinite depth lift coefficient. The presence of the free surface tends to reduce the foil's effective lift. Although sophisticated non-linear hydrofoil theory is currently being applied to foils operating near the free surface, experimental data from *Hough et al* (1969) can accurately predict the foil lift fraction, or percentage of the Prandtl solution, as a function of depth Froude number. Depth Froude number is given by expression (3.1), where d is depth below the free surface. The figure below plots the lift fraction as a function of depth Froude number for several depth over chord length ratios.

$$(3.1) \quad Fr = \frac{U}{\sqrt{gd}}$$

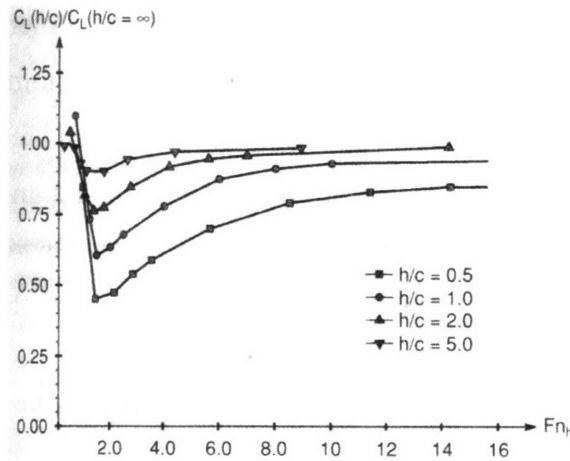


Figure 14 Fraction of Prandtl lift due to calm free surface as a function of depth Fr *Faltinsen* (2005)

To account for the presence of the free surface, the idealized Prandtl lift coefficient C_{Lreq} was increased by a lift fraction, C_{Lfrac} , interpolated from the *Hough* data. The product of the lift fraction and the idealized solution produced the effective lift coefficient, C_{Leff} . Although the Prandtl solution presumes aspect ratios significantly higher than the canard's 1.6, the idealized solution was assumed valid for the following reasons. The bow foils' effective aspect ratio is somewhat higher than geometric 1.6 due to the presence of the hull at the root chord and the "mirror image" foil on the other demi-hull. The angle of attack required, α , and the corresponding drag coefficient were given by the following expressions.

$$(3.2) \quad C_{Lreq} = \left(1 + \frac{2}{\Lambda}\right) C_{Lfrac} \quad (3.3)$$

$$C_{Deff} = \frac{C_{Lactual}^2}{\pi\Lambda}$$

Canard mounting depth d , was varied from .3m to 1.5m below the free surface in .2m increments. The following plots show the required foil angle of attack as a function of Froude number. For clarity, each hull separation ratio is presented in a separate plot.

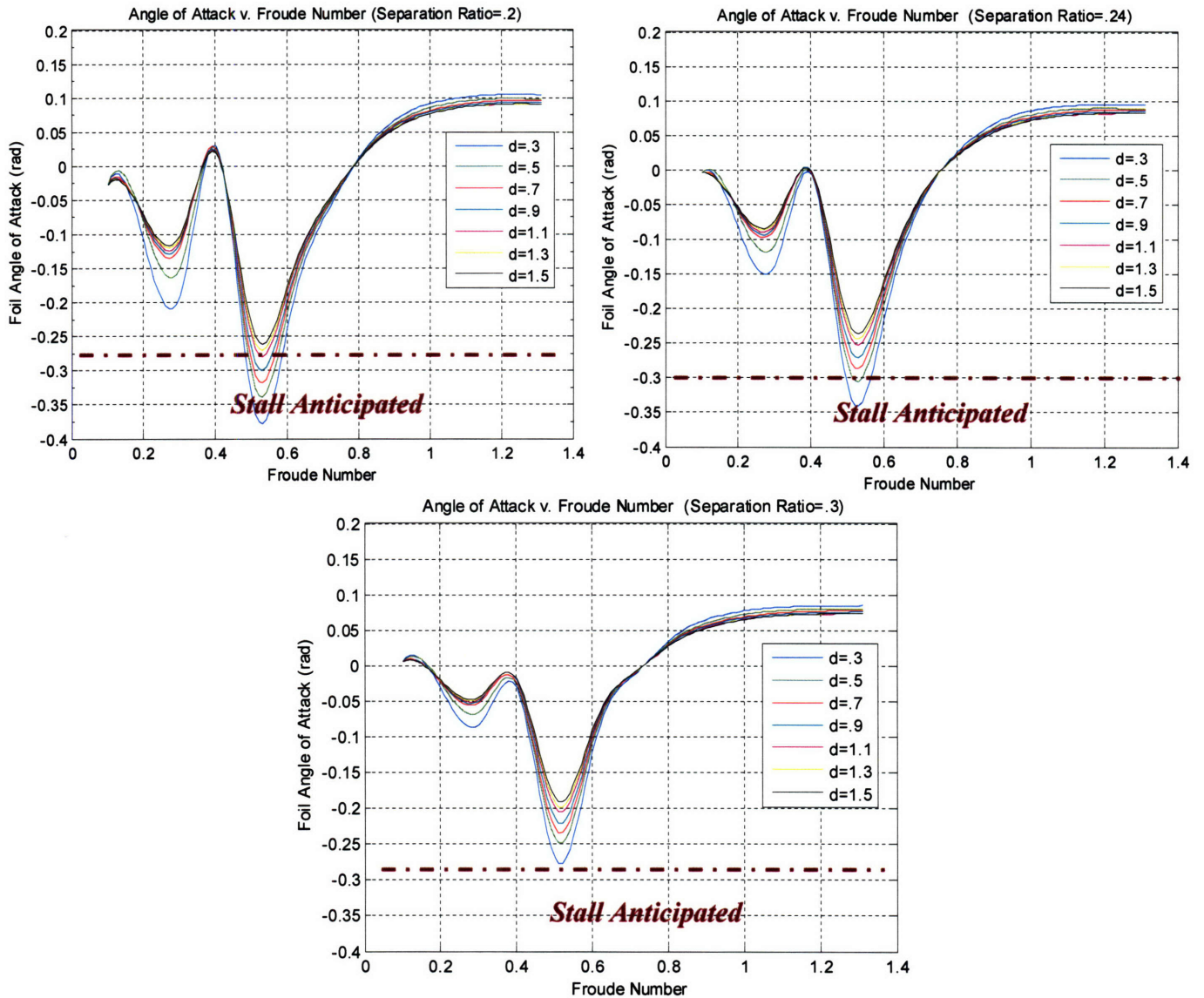


Figure 15 Required foil angle of attack for each separation ratio as a function of Fr

As expected, foils submergence and required angle of attack had an inverse relation over the entire Froude regime. The pronounced negative α at Froude number .55 is a response to bow up pre-planning behavior. The hydrodynamic pressure distribution at this speed causes the bow to rise and consequently the bow foils exert a downward force to

maintain design trim. It is anticipated that foils will stall at angles above $.28\text{rad}$ or 16° , however, angles likely to induce stall are only required for shallowly mounted foils in the $.5$ to $.6$ Froude range. Should the foils stall at this speed, the bow will move upward and is not likely to degrade performance significantly. At speeds above Froude number $.7$, all separations need an increasing positive lift force from the canards. Although the required force builds with speed, α is roughly constant because foil lift increases with velocity squared. In addition to lift, foil induced drag was predicted by expression (3.3) for each separation, speed, and depth below the free surface. The figure below presents induced drag coefficient as a function of Froude number. Once again, each separation ratio is presented in its own figure.

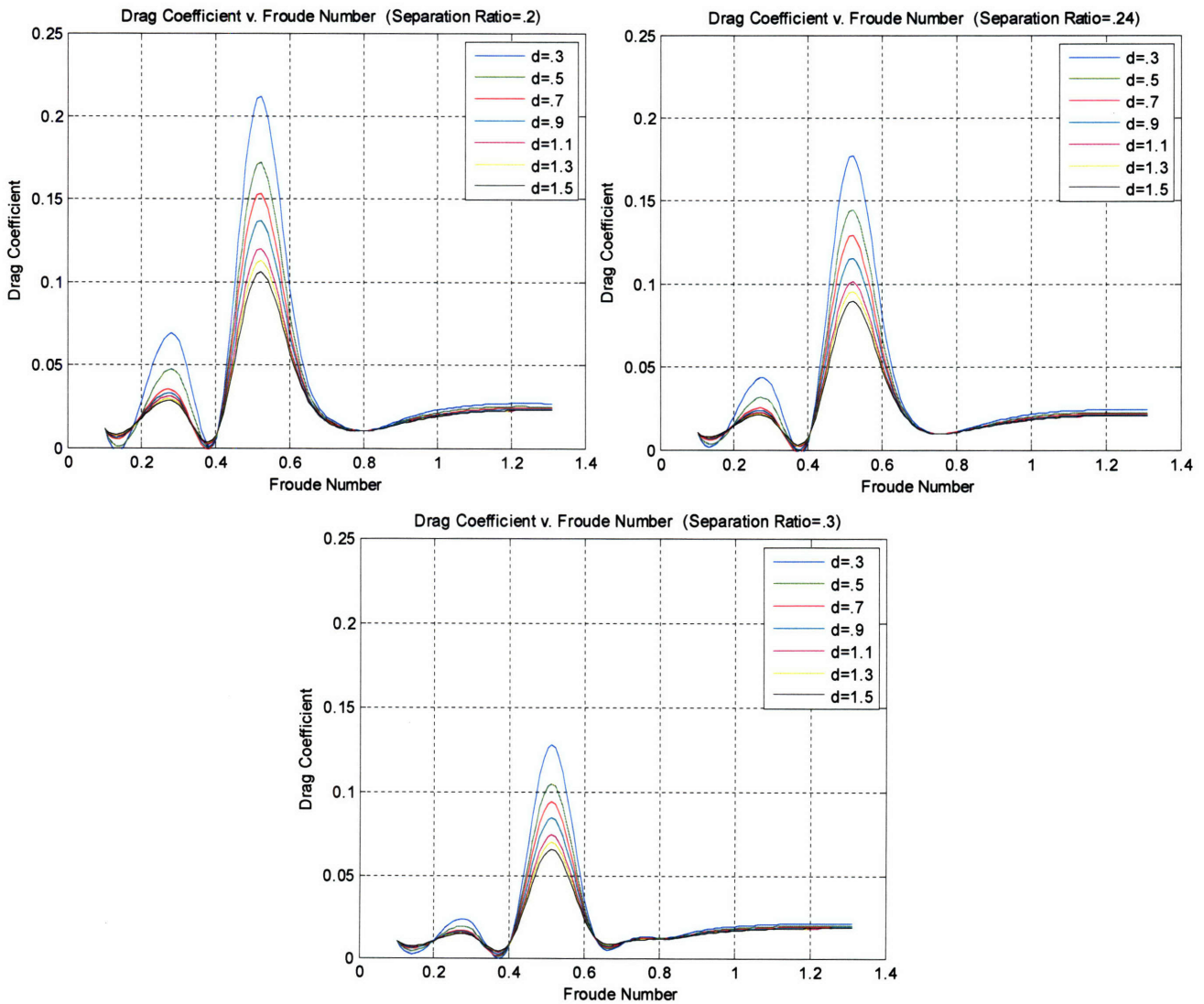


Figure 16 Drag coefficient for each separation ratio as a function of Fr

Froude number .55 shows a clear peak in induced drag coefficient for each separation ratio, speed, and depth. This result was not surprising due to the high foil loading, i.e. angle of attack, required at that speed. As was the case for bare hull resistance, narrow hull spacing exhibits the poorest behavior with high drag induced for even deeply submerged foils.

3.3 Foil Controlled Calm Water Resistance

Conventional wisdom maintains dramatic changes in displacement craft trim are a symptom, and not a cause of increased resistance. For small planing craft however, the impact of dynamic trim on drag should not be underestimated. While the round bilges of semi-SWATH make it geometrically similar to a displacement hull form, its bow up trim and decreasing draft between Froude number .4 and .6 are a clear indication of pre-planning behavior. In this Froude regime, previous studies have shown significant drag reduction can be realized by maintaining design trim through the actuation of control surfaces. Quasi-active foil control's potential resistance benefits were explored in the following section. For the all subsequent calm water foil and seakeeping foil simulations a conservative appendage mounting depth of 1.1m was selected and held constant for all separations and speeds. The following figure compares the hydrodynamic pressure experienced by the bare hull and that of the foil controlled hull underway at 22 knots.

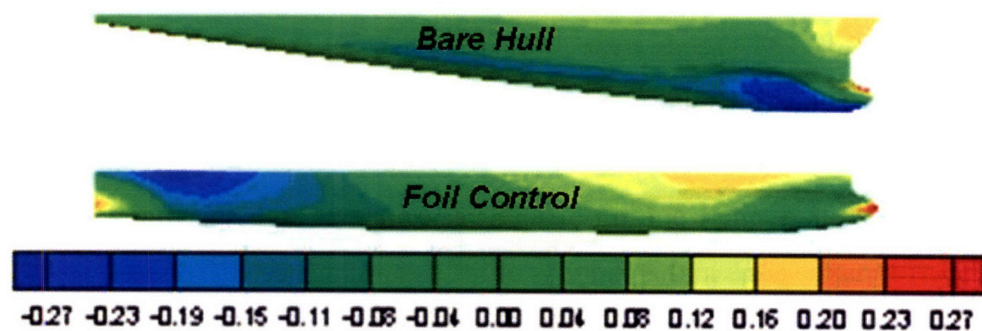


Figure 17 Bare hull & foil controlled hydrodynamic pressure at Froude number 1.2, Note improved trim and pressure distribution exhibited by the foil controlled hull.

Calm water resistance of the semi-SWATH employing quasi-active appendage control was predicted in *SWAN2* using a similar method to the one described for the bare

hull. For each run, vessel trim was set to zero and bow canard angle of attack was dialed in to produce the lift needed to make the zero trim assumption accurate. Induced resistance due to the control surfaces were added to *SWAN2*'s ideal fluid component, to arrive at the ideal drag. The following plots present ideal fluid resistance of the foil controlled hulls, as well as, the bare hull data presented in the previous chapter.

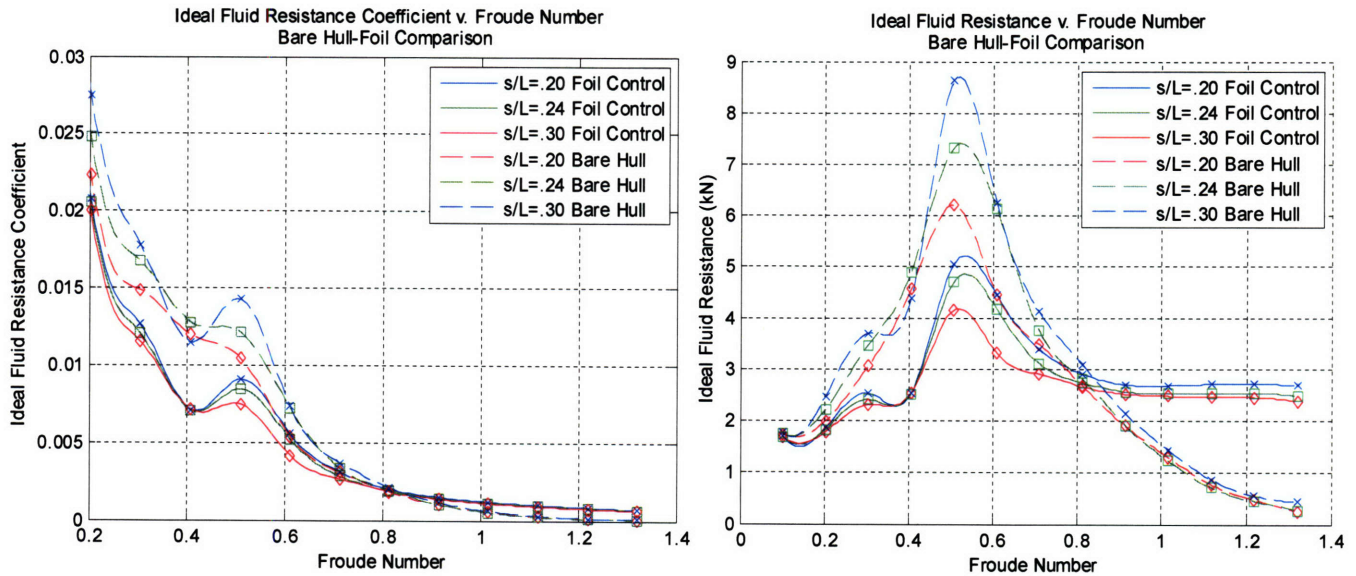


Figure 18 Ideal fluid resistance coefficient and resistance for bare hull & foil controlled hull

Figure 18 reveals a substantial drag reduction in foil controlled hulls at speeds below Froude number .8. This is particularly true at the critical .55 Froude number, at which the peak resistance was decreased by an astounding 35%. While increased hull separation once again exhibited superior performance, its effect was less pronounced than for the bare hull. At speeds over Froude number .8, the bare hull showed slightly less resistance than the foil controlled vessel. This is because the ideal fluid resistance is dominated by foil induced drag in this speed range. As shown later in this chapter, ideal fluid resistance is a small portion of total resistance at high-speed and therefore the bare hull's performance edge in this range is of little consequence.

As previously discussed, the viscous resistance can be up to four times greater than the ideal fluid resistance at high speeds. The viscous resistance of the foil controlled vessel was predicted using the method described earlier for the bare hull. Twice the planform area of each foil was added to the hull wetted surface area to include the frictional resistance of the foil in the total viscous resistance.

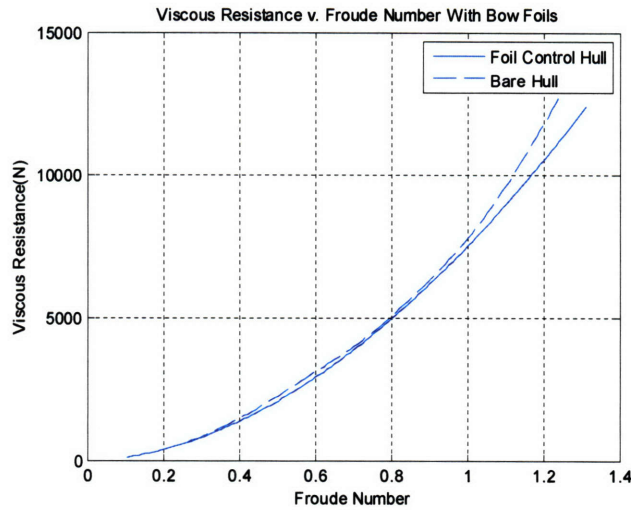


Figure 19 Viscous resistance as a function of Fr

The figure above indicates that at speeds above the critical .55 Froude number, the foil controlled hull experienced a slightly lower viscous resistance than the bare hull and is due to a lower wetted surface area. Despite the additional foil wetted surface area, the bare hull wetted surface area is larger at high speeds due to its pronounced trim by the bow.

Finally, the total resistance was calculated for each separation in the foil controlled configuration. Total resistance and resistance coefficient were determined by adding the viscous resistance, including form effects and ideal fluid resistance presented in Figure 18.

The following figure presents these results along with bare hull results from Chapter 2.

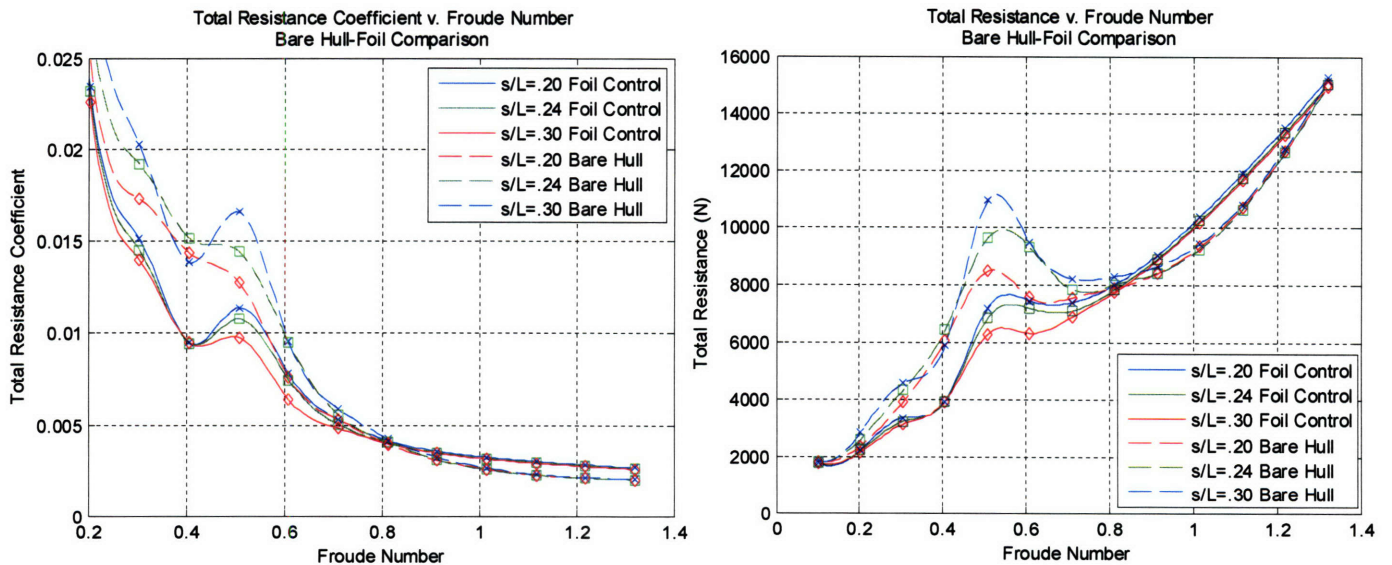


Figure 20 Total resistance coefficient and resistance for bare hull and foil controlled hull

Consistent with the ideal fluid resistance predictions, the hulls employing the quasi-active foil control systems showed a significant reduction in total resistance below Froude number .8. By actuating bow canards to generate the appropriate amount of lift, the unfavorable pressure gradient near the bow, and resulting *Munk Moment*, was equilibrated and design trim maintained. The resulting improved pressure distribution around the hulls seen in Figure 17 produced significant improvement in overall performance. A reduction in total resistance was achieved in spite of additional foil wetted surface and foil induced drag. Comparing Figure 19 and Figure 20, it is clear that ideal fluid resistance dominates around the critical Froude number .55. In reducing this resistance component by approximately 35%, foil control smoothes the resistance hump resulting in a more conventional resistance plot. Foil control also appears to reduce adverse interaction between narrowly spaced demi-hulls with separations nearly indistinguishable from one another in Figure 20. From Froude number .8 to 1.3, the bare hull exhibits a slightly lower resistance due to its lack of induced foil resistance. Noting the slopes of the resistance curves at Froude number 1.3, it is plausible to assume the foil controlled vessel will exhibit lower total resistances at speeds above this speed.

Unequivocally, the data presented in this chapter suggests each hull separation ratio benefited from quasi-active, speed actuated control surfaces. This was especially true at cruising forward speeds between 8 and 16 knots. The dynamic trim produced larger high-speed bare hull operation was outside the realm of practicality for vessel design and therefore it is likely that if built, the semi-SWATH will have a speed actuated system similar to the one used in this analysis. In addition to providing resistance benefits, the improved trim angle and passive foil damping is thought to improve seakeeping performance and is explored in Chapter 5.

Chapter 4: Bare Hull Seakeeping Response

4.1 Introduction

Vessel seakeeping, or the motions exhibited by a ship due to the presence of surface waves, has become increasingly important in recent years. Several factors have driven the study of ship motions to the forefront of naval architecture. The first of which is the expanding use of high-speed semi-displacement craft. Even while underway at high speeds, these ships are expected to provide a safe environment for passengers or delicate onboard systems. There is also growing sentiment from the operators, regulatory bodies, and the public at large to ensure safety at sea for passengers and crew *Couser* (2000). Lastly, the recent development of accurate analytical motion simulation tools has made seakeeping prediction possible for even for these advanced marine vehicles.

While of importance to all ocean-going vessels, the performance of new high-speed, light displacement craft is dramatically altered by operation in surface waves. As a general rule, the importance of seakeeping increases with forward speed. The large hydrodynamic pressures and momentum coupled with high impulsive forces exerted by waves, creates the potential for great accelerations and the structural loading. Predicting these accelerations is the first step to a means of suppressing them and is central to the design of any high-speed craft.

Seakeeping analysis, or prediction of vessel motion, is traditionally separated into three distinct parts. The first is the estimation of likely environmental conditions to be encountered by the vessel. These conditions are described by mariners as a sea state, or mathematically by an ambient wave spectrum. The second and most difficult part of the problem is the prediction of vessel motions in a seaway. Finally, the vessel's response is compared to established criteria for the ship's intended use. Motion criteria codes like the IMO HSC limit peak RMS accelerations to improve passenger comfort and ensure

continuous operation of sensitive shipboard equipment. A comparison of the semi-SWATH response to such criteria is beyond the scope of this study.

The seakeeping response of the semi-SWATH in heave, pitch, and roll are presented in the following chapter. Of the remaining motions, surge is typically neglected and the sway and yaw response are included *Appendix B: Sway and Yaw Response*. Once again, the time domain, computational fluid dynamics code, *SWAN2* was used in predicting motions. The three demi-hull separation ratios studied in calm water were again used to gauge separation's influence on seakeeping. The speed range was narrowed to include only "cruising speeds" of 10 to 20 knots. Vessel operating conditions were simulated by using single monochromatic waves of constant amplitude and variable modal frequency. Wave frequency was varied to correspond to relevant non-dimensional wavelengths, or wavelength over waterline length, λ/L_{wl} . Although an irregular sea state is more accurately described by the linear superposition of many waves, fully developed seas tend to be narrowly banded in frequency and have a single dominate wave height. This uniformity makes a single unidirectional wave of modal frequency a reasonable description of ambient waves. *SWAN2* was used to simulate semi-SWATH response in several wave headings over the cruising speed range.

4.2 Heave, Pitch, and Roll Response

This section presents the heave, pitch, and roll motions of the semi-SWATH operating in a seaway. For consistency with the calm water study, separation ratios were again set at $s/L=0.20$, $s/L=0.24$, and $s/L=0.3$. The bare hull dynamic sinkage and trim found in Chapter 2 were input into *SWAN2* to isolate incident wave response from steady dynamic effects. The response of each separation was evaluated at six speeds from Froude number .5 to 1 in 2 knot steps. Each simulation was run for three wave headings corresponding to head, port-bow, and beam seas. These incident wave angles are defined by *SWAN2* as $\beta=180^\circ$, 135° , and 90° measured with respect to the negative x-axis. That is to say, following and quartering seas approach the ship from abaft the beam have a β between 0° and 90° , while head and port-bow seas have angles between 90° and 180° . Accordingly, beam waves, or those moving perpendicular to forward motion, are

characterized by $\beta=90^\circ$. The following figure defines heave, pitch and roll motions of a monohull in the internal *SWAN2* coordinate.

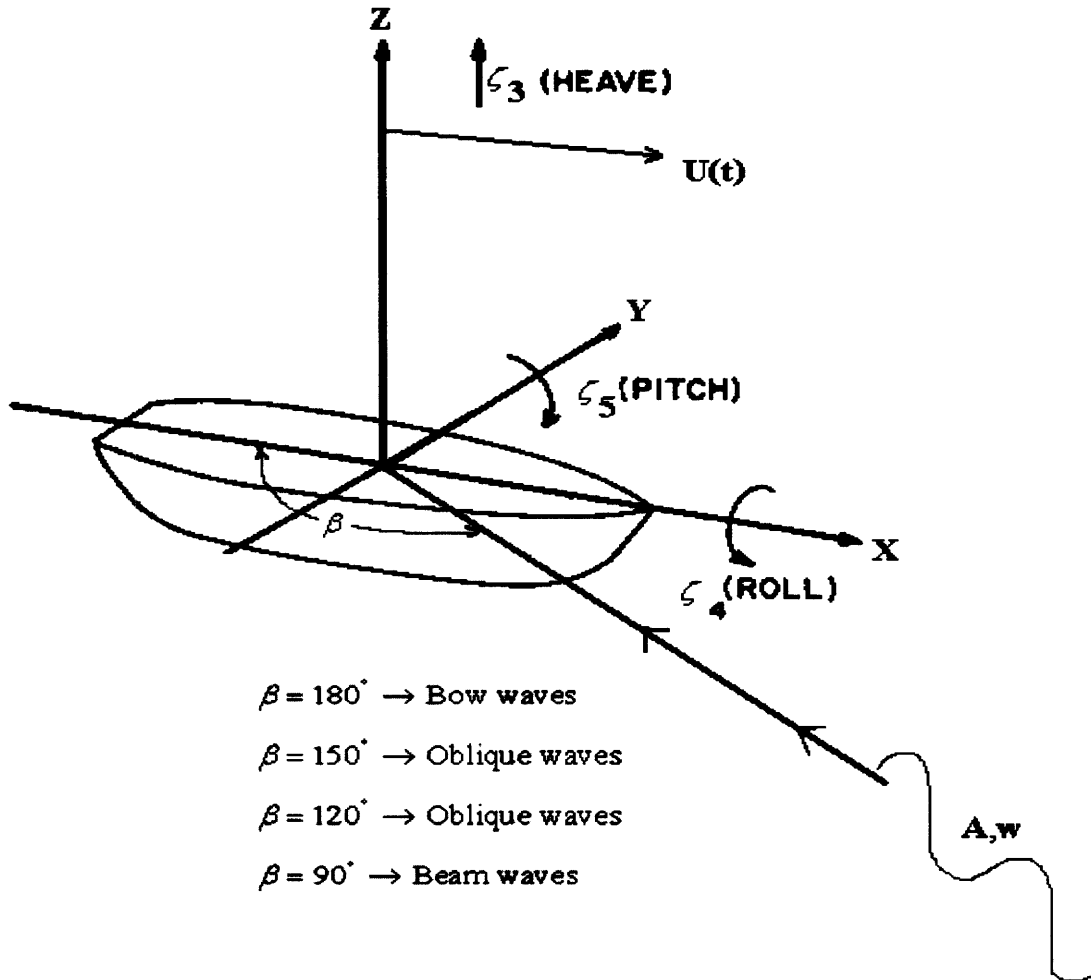


Figure 21 *SWAN2* coordinate and motion definition *Purvin* (2003)

As is common in seakeeping study, vessel response was quantified in terms of a response amplitude operator, or RAO, for each mode of motion. Defined as the ratio between the response modulus and incident wave amplitude, the RAO is a widely used means of non-dimensionalizing vessel response. The ship response amplitude is measured by *SWAN2* at the origin of its internal coordinate system and is dependent on wave encounter frequency. Encounter frequency is given by the expression (4.1) where U is the forward vessel speed and w is the absolute wave frequency as seen by a stationary observer on the beach.

$$(4.1) \quad w_e = w - \frac{w^2}{g} U \cos \beta$$

The incident wave height for all simulations was fixed at 1m. As previously discussed, wave frequencies were selected to correspond to relevant non-dimensional wavelengths ranging from .1 to 7. Over most of this range, vessel response was sampled at a λ / L_{wl} increment of .2, but the step size was adjusted according to the second derivative of the RAO. This process dictated more frequent measurement near peak response and fewer where the response was more linear. The figures in this chapter plot heave, pitch, or roll RAO in units of (m/m) for motions along a body fixed axis as in heave, or (m/deg) for rotation about an axis as in pitch and roll, versus non-dimensional wavelength, λ / L_{wl} .

4.2.1 Head Seas Seakeeping Response

The following figure is a snapshot of the 18 knot seakeeping simulation for the 0.24 separation ratio in head waves with a 3 second period and wave height of 1m.

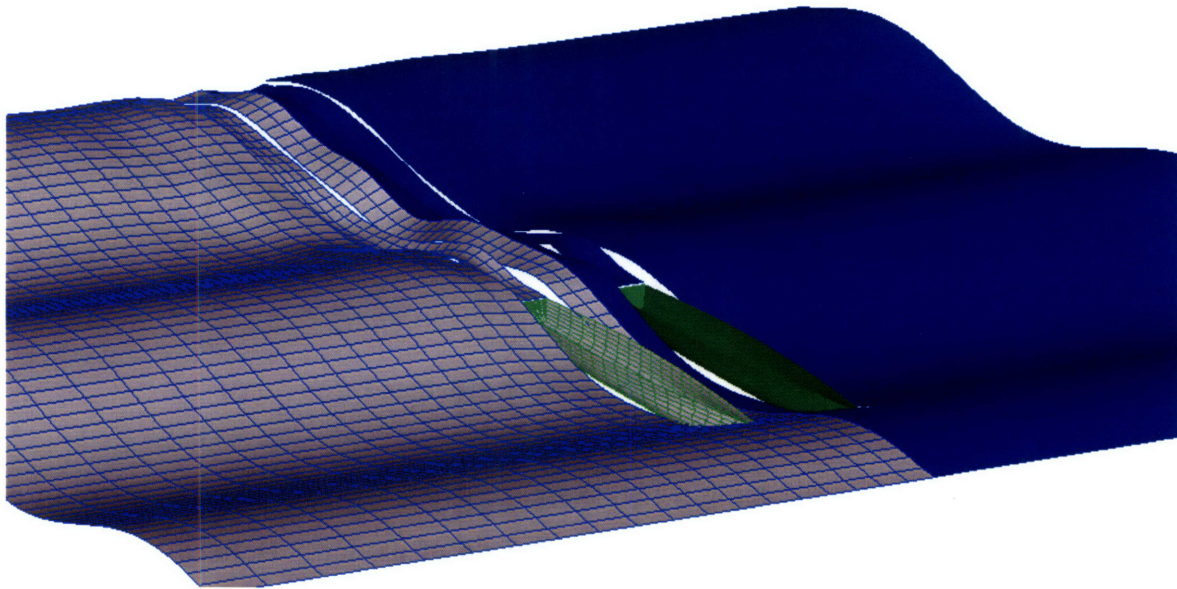


Figure 22 Semi-SWATH seakeeping simulation in head seas at 18 knots, Note: Only hull surface below the mean free surface is shown.

Figure 21 presents the heave motion RAO for each separation ratio in head waves, or $\beta=180^\circ$. The semi-SWATH was examined at six different speeds forward speeds from Froude number .5 to 1.0 with the response of each demi-hull separation ratio shown on a separate plot.

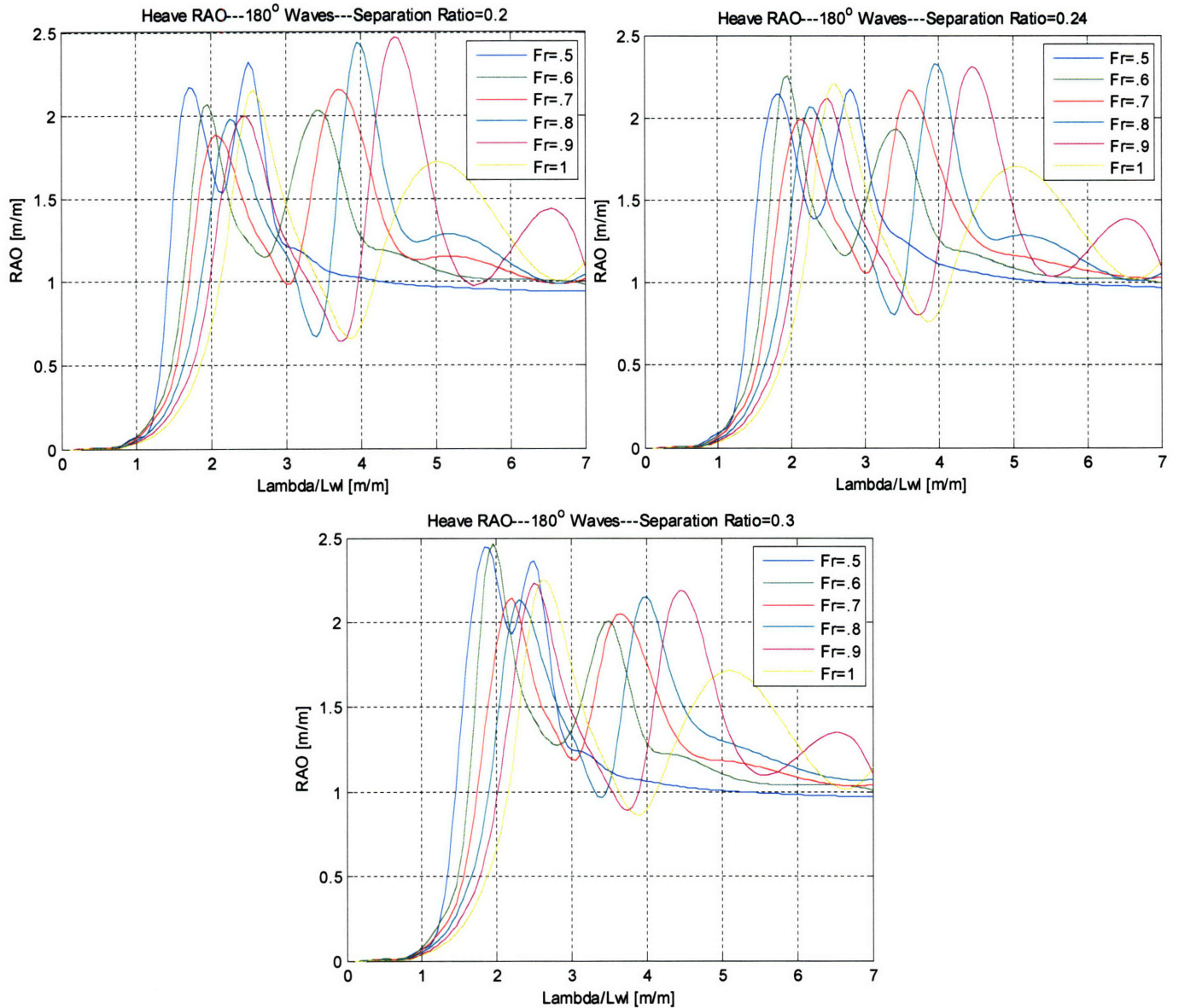


Figure 23 Heave RAO in head seas for each separation ratio

The heave response above clearly shows two distinct RAO peaks of roughly equal magnitude for each forward speed. Large demi-hull interactions coupled with impractical trim angle are a likely cause of dual response maxima. Each local maximum represents a resonant wave encounter frequency at which a relatively small wave input produces significant vessel motion. The amplitude of heave decreases slightly with increasing forward speed suggesting a slight improvement in seakeeping at higher forward speeds. The frequency and amplitude of maxima response does not appear to be dependent on separation ratio with each plot showing a similar response. As speed increases, vessel resonance is excited by increasingly longer wavelengths, i.e. peaks move to the left. It is

likely these longer wavelengths are required to match a single set of resonant encounter frequencies. As anticipated, wavelengths exceeding five times the waterline length produce RAO's tending to unity. In other words, a 1m high wave produces exactly 1m of heave response. This indicates wave contouring behavior in which the vessel length becomes insignificant when compared to wavelength and the vessel behaves increasingly like a single point on the ambient waves. For relatively short waves, $\lambda / L_{wl} = 1.5$ to 0, the wave excitation frequency becomes too fast to induce vessel response, and consequently response amplitude tends to zero. Heave is not the only mode of motion excited by head waves. Of equal or greater importance is semi-SWATH pitch response. The following figure presents the pitch response for each separation ratio operating in head seas.

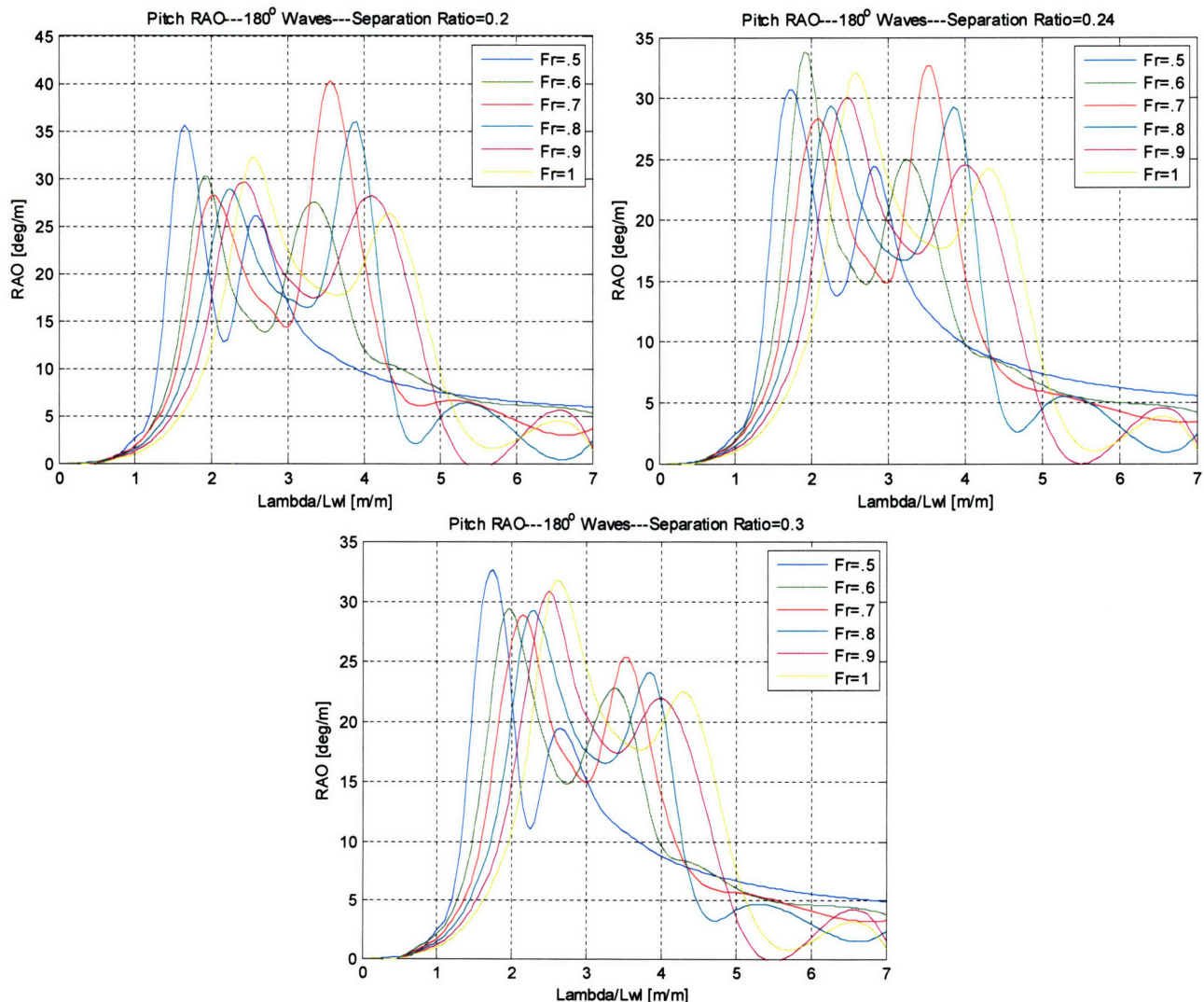


Figure 24 Pitch RAO in head seas for each separation ratio

The semi-SWATH pitch response in Figure 24 shows two distinct RAO peaks of roughly equal magnitude at each forward speed. Like heave response, demi-hull interactions and large trim angles obscure the conventional single resonant frequency response in pitch. A minor improvement is shown for the largest separation ratio 0.30. For all separation ratios however, the vessel appears to be quite sensitive, or tender, in pitch with peak RAO's exceeding $35^\circ/\text{m}$. This result was unexpected as the semi-SWATH's small waterplane forward was designed to decouple wave elevation from pitch and thereby reducing motion. The large dynamic trim discussed in the previous chapters forces the vessel's flared bow into contact with waves and therefore dramatically increases the waterplane area forward. Maintaining design trim is thought to significantly improve overall seakeeping behavior and is examined in Chapter 5.

Peak pitch response occurred in the λ/L_{Lwl} range of 1.5 to 4, and tended to decrease with increasing Froude number to .7, then increased with speed thereafter. Once again, small wavelengths produced variation in excitation force too fast for the vessel to respond while larger wavelengths reflected wave contouring with RAO's tending to the wave slope. As intuition predicts, roll motion is not excited by head seas and therefore is not be presented for $\beta=180^\circ$.

4.2.2 Beam Seas Seakeeping Response

The bare hull seakeeping response of each separation ratio in beam seas, $\beta=90^\circ$ is presented below. The following figure is a snapshot of the 18 knot seakeeping simulation for the 0.24 separation ratio in beam seas with a 3 second period and wave height of 1m.



Figure 25 Semi-SWATH seakeeping simulation in beam seas at 18 knots

Figure 26 presents the heave motion RAO for each separation ratio in head waves, $\beta=180^\circ$. The semi-SWATH was examined at six different speeds forward speeds from Froude number .5 to 1.0 with the response of each separation shown on a separate plot.

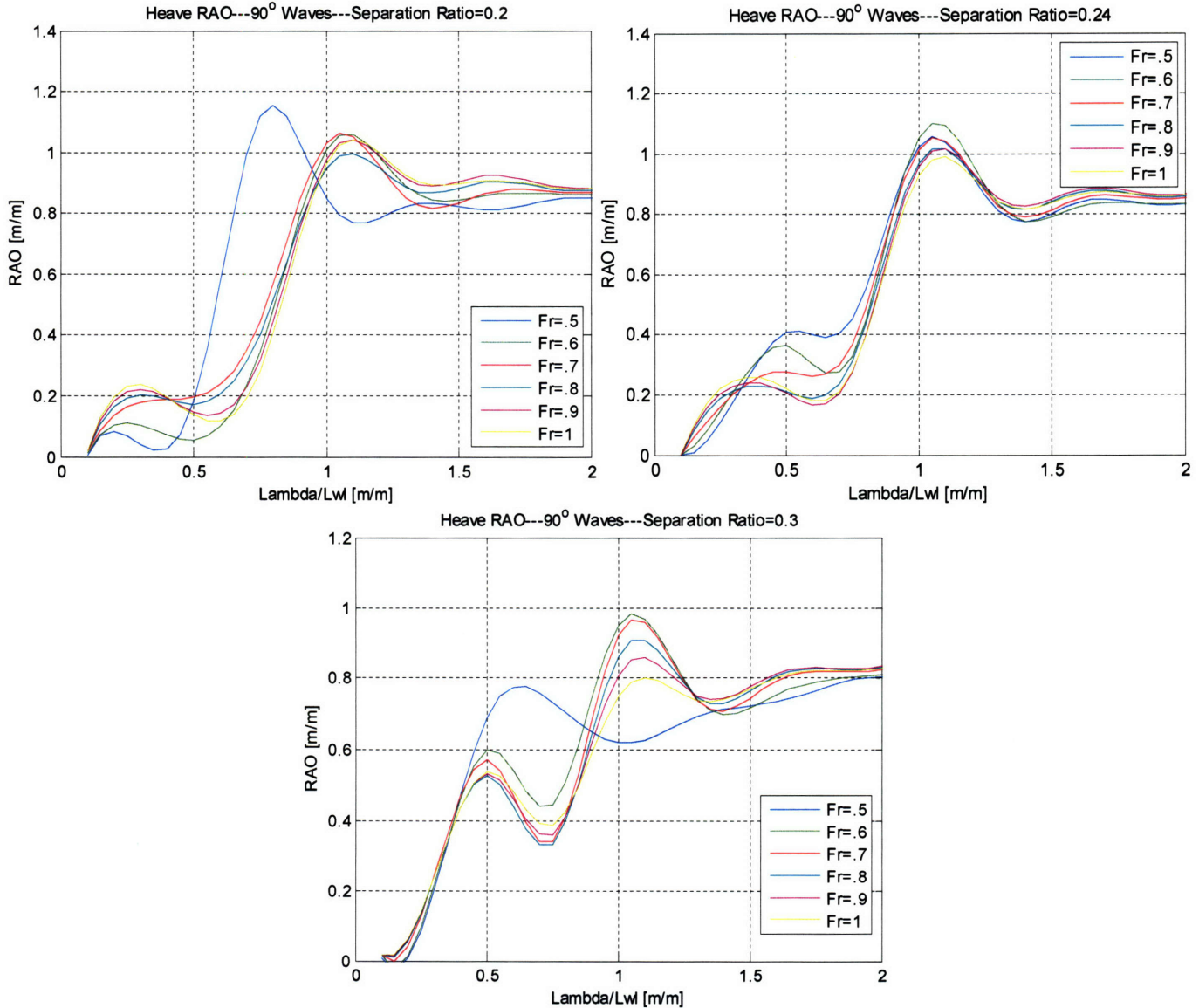


Figure 26 Heave RAO in beam seas for each separation ratio

The heave RAO plots in Figure 26 show several general trends. First is the semi-SWATH's general stiffness, or insensitivity, in heave to beam wave excitation. Peak response amplitudes were only slightly greater than unity. Resonant response for all separation ratios occurred in the $\lambda/L_{wl} = .5$ to 1.24 range, which is a factor of 2 less than the range exciting significant response in head seas. Reduction in relevant wavelengths is attributed to the fact that the hull dimension of interest is overall vessel beam and not

waterline length. A more appropriate definition of non-dimensional wavelength in beam seas might be wavelength over waterline beam, or λ/B_{Lwl} . Such a redefinition would likely produce resonance in similar non-dimensional wavelengths to those observed in head seas. The maximum amplitude of the response decreased with increasing hull separation due to the corresponding increase in overall waterline beam. It is interesting to note the heave response tends to .85 and not 1 for wavelengths significantly larger than the total beam. Clearly the demi-hulls are contouring to the free surface, but because the hulls are separated by a nontrivial distance, both demi-hulls are never on single wave crest at the same time. Therefore, even when following the surface of 1m high wave, the peak heave displacement was only .85m. Bringing hull separation to zero, i.e. creating a monohull, would push heave RAO to unity as seen in head waves. The following plots show semi-SWATH pitch response in beam seas.

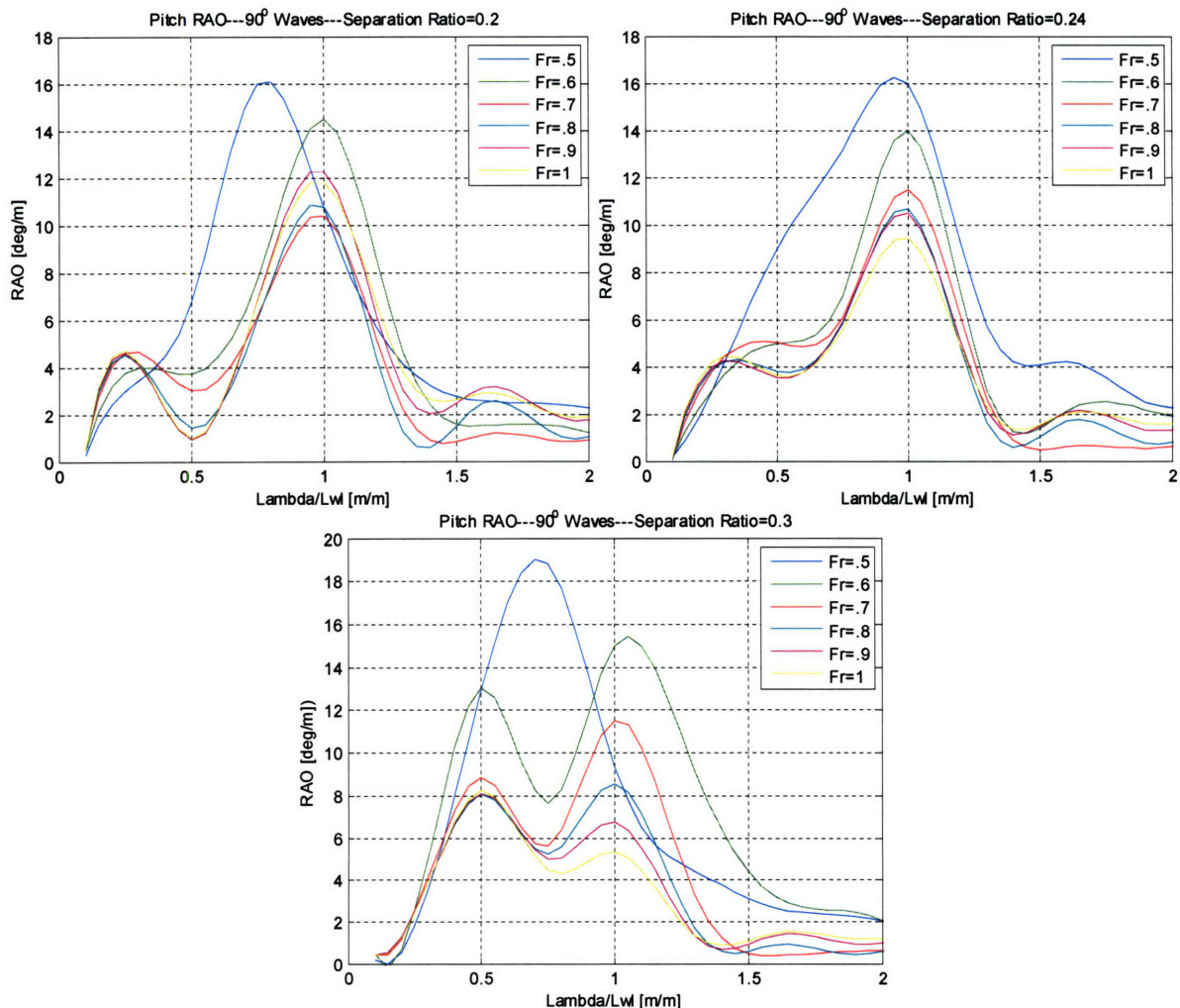
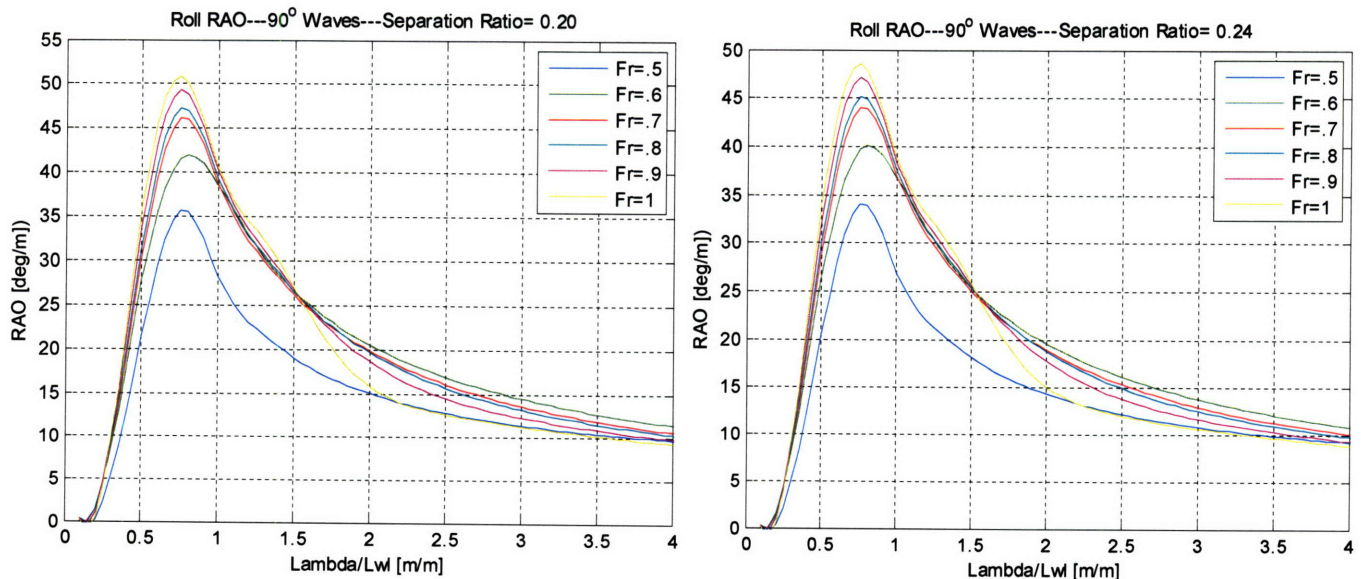


Figure 27 Pitch RAO in beam seas for each separation ratio

The RAO plots in Figure 27 demonstrate surprisingly large pitch motions with peak RAO's exceeding $16^\circ/\text{m}$. The pitch sensitivity to beam waves is due to the high degree of fore and aft asymmetry of the semi-SWATH demi-hull. The waterplane area aft of amidships is roughly a factor of 2 greater than waterplane forward. The resulting volumetric imbalance induces hydrostatic coupling between roll and pitch and accounts for the exaggerated beams seas pitch motion. In general, response diminishes with larger forward speeds and unlike modes previously discussed, there appears to be no seakeeping advantage to increasing demi-hull separation.

Typically greatest in magnitude, and hence importance, roll response in beams seas is of great interest to the semi-SWATH designer. For most vessels, the magnitude and frequency of these accelerations correspond to those of maximum human sensitivity and are likely to produce sea sickness and onboard system malfunction. If large enough, roll oscillations may even threaten transverse stability of the vessel and result in capsize. Although typically of less concern for catamarans, large roll motions are facilitated in all vessels by the smaller waterplane moment of inertia in the transverse direction and associated hydrostatic righting moment. In addition to the weak restoring force, the round bilge turns of the semi-SWATH produce fewer radiated waves than a hard chined vessels, resulting in less radiated wave damping. The consequence of a weak restoring and damping is a greater sensitivity to resonant effects. The following plots present roll response of each separation operating in beam seas.



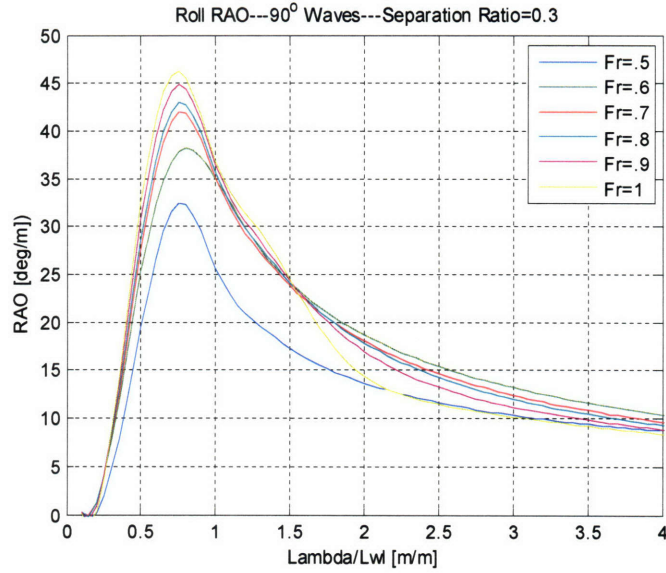


Figure 28 Roll RAO in beam seas for each separation ratio

The plots in Figure 28 show a well-defined resonant response with peak RAO's of approximately $45^\circ/\text{m}$. Large amplitude motion was excited by a constant $\lambda / L_{Lwl} = .75$ for each separation ratio over the entire speed range. This wavelength corresponds to roughly two times the overall beam as shown in Figure 29. Forward speed had no effect on this critical wavelength because forward speed does not affect encounter frequency when $\beta=90^\circ$. The amplitude of the response is however, dependent on speed and separation ratio. For all separations, increased forward speed generated larger motions. Reducing speed from 20 to 10 knots reduced roll RAO by approximately 30%. Larger separations produced smaller roll motions over all forward speeds. Increasing the separation ratio increases overall beam and consequently waterplane moment of inertia. The resulting increase in hydrostatic righting moment produces a stiffer dynamic system that is less responsive to wave input at the resonant encounter frequency of $\lambda / L_{Lwl} = .75$.

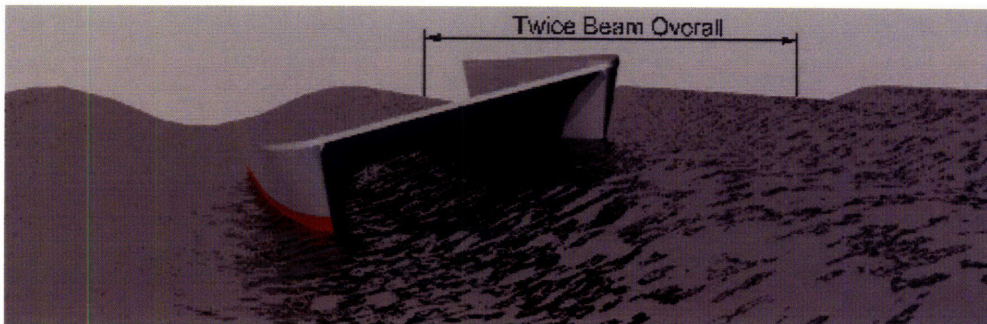
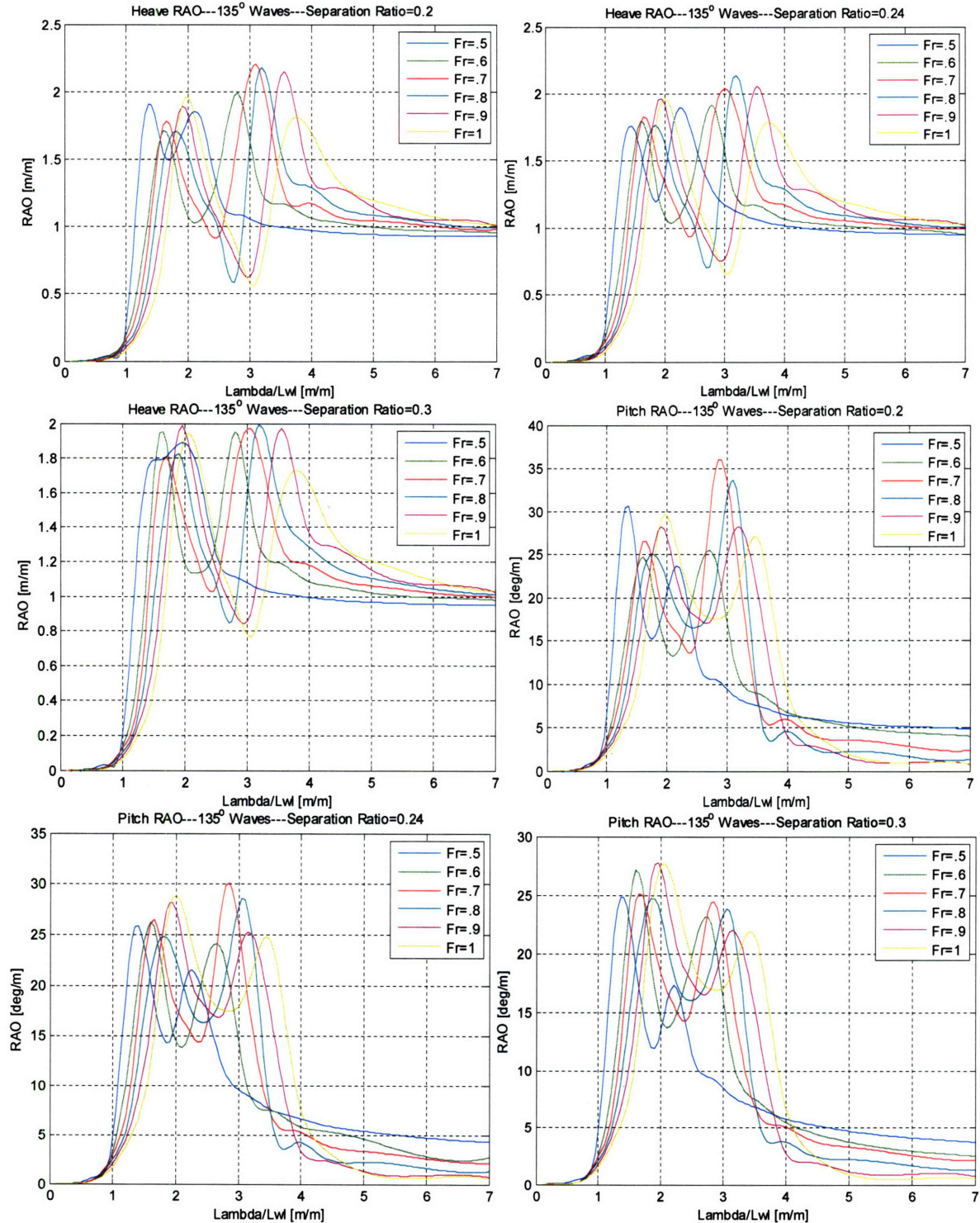


Figure 29 Semi-SWATH in resonant beam seas where $\lambda / L_{Lwl} = .75$

4.2.3 Port-Bow Seas Seakeeping Response

The bare hull seakeeping response of each separation ratio in port-bow seas, or incident wave angle $\beta=135^\circ$, is presented below. Due to the semi-SWATH's port-starboard symmetry, the $\beta=135^\circ$ simulation prediction of response starboard bow.



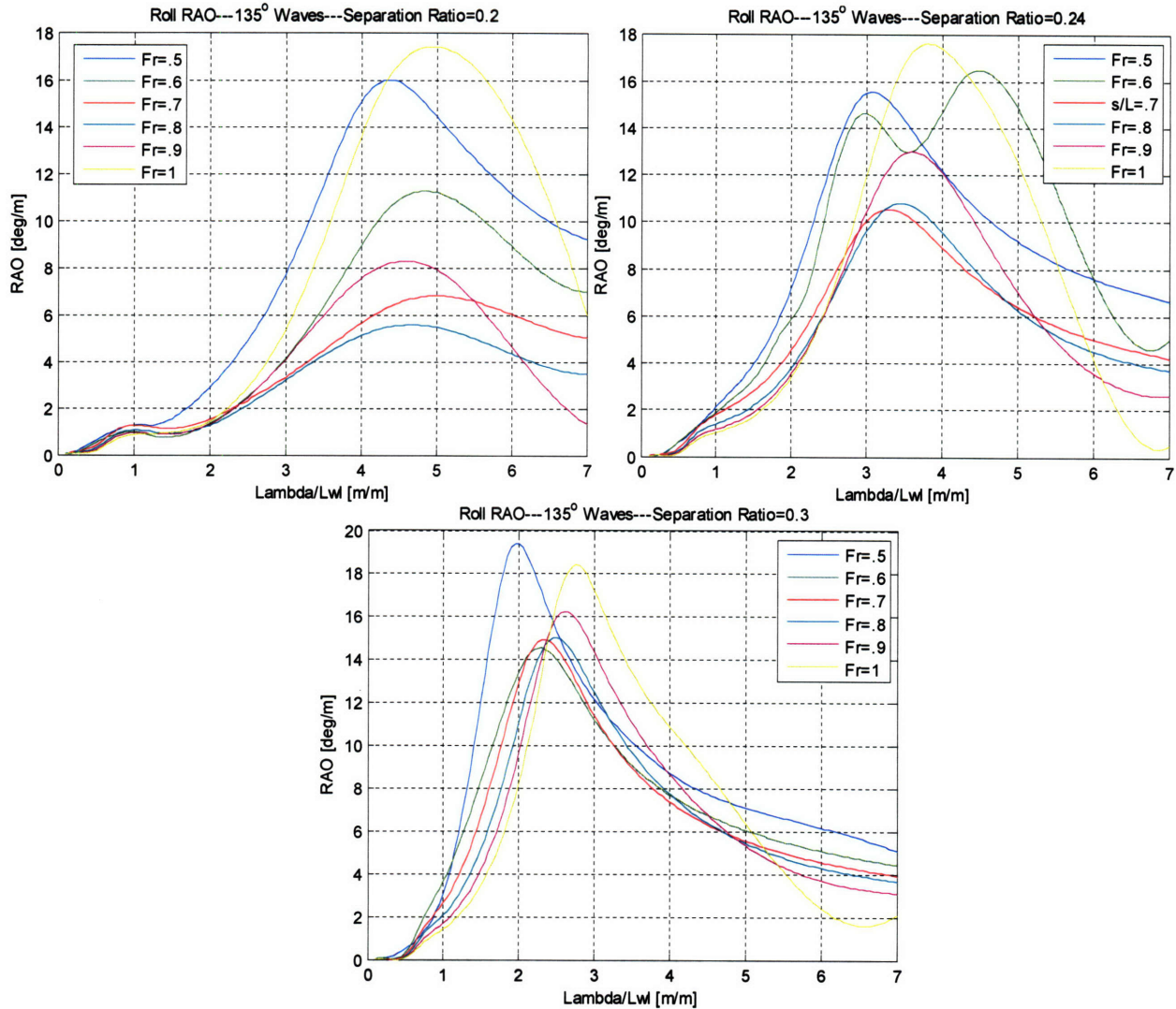


Figure 30 Heave, Pitch, and Roll RAO in $\beta=135^\circ$ seas for each separation ratio

Operating at forward speeds corresponding to Froude number =.5 to 1.0, in ambient waves off the port or starboard bow, the simulations predict similar vessel response to the beam and head seas. Pitch and heave plots in **Error! Reference source not found.** once again show dual resonant peaks of roughly equal amplitude. The likely reason is hydrodynamic hull interaction and the unrealistic operating trim angles. As expected, the roll response shows smaller amplitude oscillations than $\beta=90^\circ$, but like beam seas, suggests a reduction in motion with lower forward speed.

Chapter 5: Foil Controlled Seakeeping Response

5.1 Introduction

In addition to the calm water resistance benefits of the quasi-active canard system discussed in Chapter 3, control surfaces have been shown to provide important passive damping in heave, pitch and roll. Foils located near the bow are particularly effective at reducing heave and pitch motions due to the large vertical motions experienced by the bow. These undesirable accelerations create a time varying angle of attack on the canards that must be added to the steady angle actuated to correct trim instability. Provided the new angle of attack does not induce stall, the altered inflow produces a lift force opposing vertical motion. This damping force increases linearly with forward speed making this system well suited for use on high-speed semi-SWATHs.

5.2 Foil Controlled Heave, Pitch, and Roll Response

With shape and amplitude of bare hull response known, seakeeping performance of the semi-SWATH with quasi-active foil control was examined. The lifting appendages used were identical in shape and mounting location to those used in the resistance evaluation. The steady angle of attack of each foil was adopted from the calm water study and was the precise angle needed to maintain zero trim at each speed. Unlike the resistance study, only the “as designed” separation ratio of 0.24 was evaluated. Vessel response was measured at six speeds from Froude number .5 to 1. Once again, each simulation was run for wave headings corresponding to head, port-bow, and beam seas. These incident wave angles are defined by *SWAN2* as $\beta=180^\circ$, 135° , and 90° measured with respect to the negative x-axis as shown in Figure 21. The incident wave height for all simulations was a constant 1m. As previously discussed, wave frequencies were selected

to correspond to relevant non-dimensional wavelengths ranging from .1 to 7. Vessel response was sampled at λ / L_{wl} increment of .2, but was adjusted according to the rate of change of the response. Vessel motions were predicted by *SWAN2* and quantified in terms of the response amplitude operator, or RAO, corresponding to each non-dimensional wavelength. RAO's were extracted from code output and presented in the following sections.

5.2.1 Head Seas Seakeeping Response

The following figure presents the heave and pitch response of the semi-SWATH operating at variable forward speed in head waves.

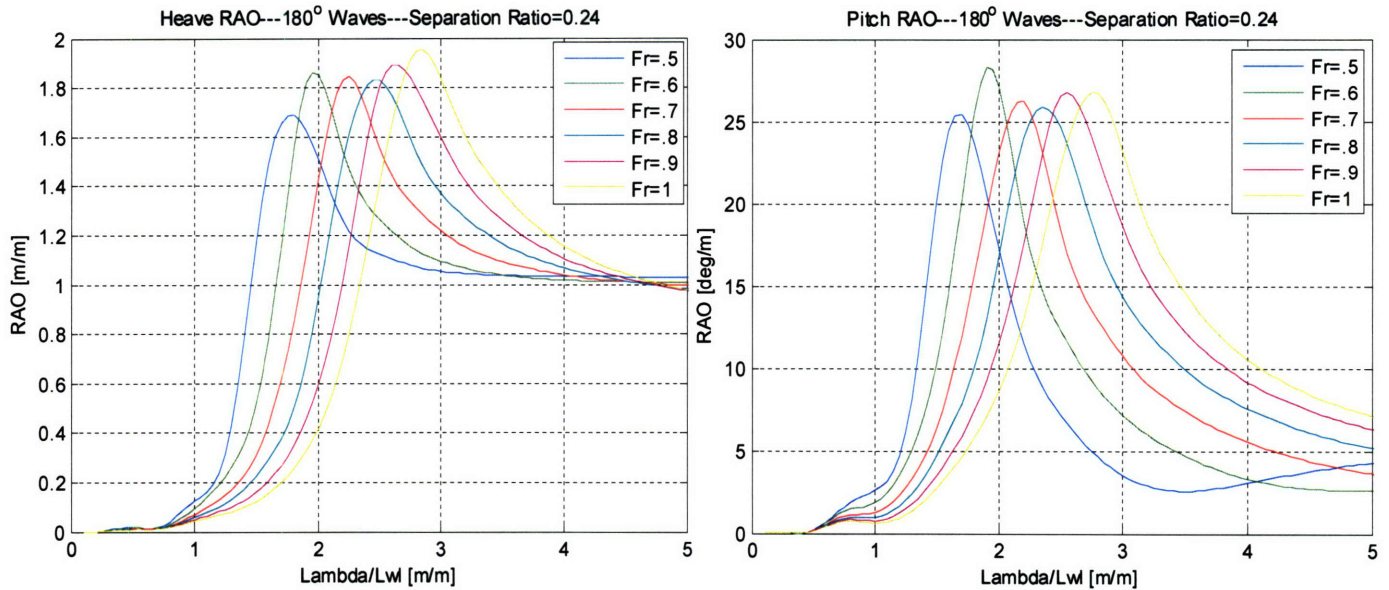


Figure 31 Foil damped Heave & Pitch response in head seas for each separation ratio

The plots in Figure 31 show a clearer, more conventional single resonant heave response. Correcting dynamic trim instability produced an improved pressure distribution particularly near the bow and reduced adverse demi-hull interactions that create the dual response maxima present in bare hull simulations. Once again, as forward speed increases, resonance was excited by progressively longer wavelengths. It is assumed all of the peak wavelengths correspond to a single resonant encounter frequency. Large non-dimensional wavelengths produced RAO's tending to unity indicating wave contouring. Extremely small wavelengths produced a wave excitation frequency too rapid to induce vessel

response, and therefore amplitude tended to zero. Heave increased slightly with greater forward speed suggesting a slight improvement in seakeeping at lower forward speeds.

Of greater importance to operation in head seas, $\beta=180^\circ$, is vessel pitch response. Like the foil controlled heave response, Figure 31 shows a clearer, more conventional single resonant λ/L_{Lwl} for each speed. Largest pitch oscillations were observed in 1.5 to $3.0\lambda/L_{Lwl}$ ranges, i.e. those corresponding to 1.5 to 3 times the vessel waterline length. Conventional high-speed catamarans in head seas typically exhibit pitch resonance in shorter waves, λ/L_{Lwl} 1.3 to 2.25. The plot below illustrates a typical 100m high-speed semi-displacement catamaran's pitch response in head waves. Note the all resonant peaks occur at non-dimensional wavelengths of less than 2.25, i.e. peaks shift left when compared semi-SWATH response.

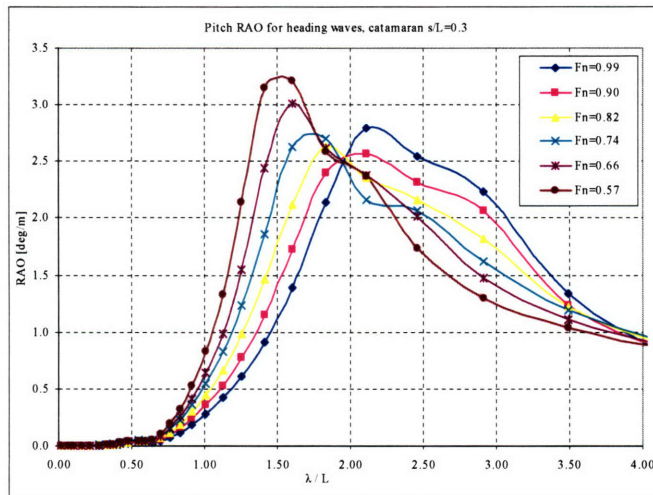


Figure 32 Conventional high-speed catamaran pitch response in head seas Purvin (2003)

The semi-SWATH requiring longer waves, i.e. lower encounter frequencies, to produce large oscillations is not surprising. It is well established that semi-submersibles have lower resonant frequencies than conventional vessels. Although the peak response is larger in amplitude than the catamaran response shown above, largely due to scale effects, semi-SWATH resonant phenomena were restricted to a narrow-band of the wavelength regime. In other words, at a given forward speed, large amplitude motions only occur within a small range of wavelengths, whereas the high-speed catamaran is sensitive to a much wider array of seas. Like heave response, a slight increase in oscillation is observed with increasing forward speed.

5.2.2 Beam Seas Seakeeping Response

The quasi-active foil controlled seakeeping response of the 0.24 separation ratio in beam seas, $\beta=90^\circ$ is presented below. Figure 33 presents the heave, pitch and roll motion RAO for the “as designed” separation ratio. Once again, the semi-SWATH was examined at six different speeds forward speeds from Froude number .5 to 1.0 with each mode of motion shown on a separate plot.

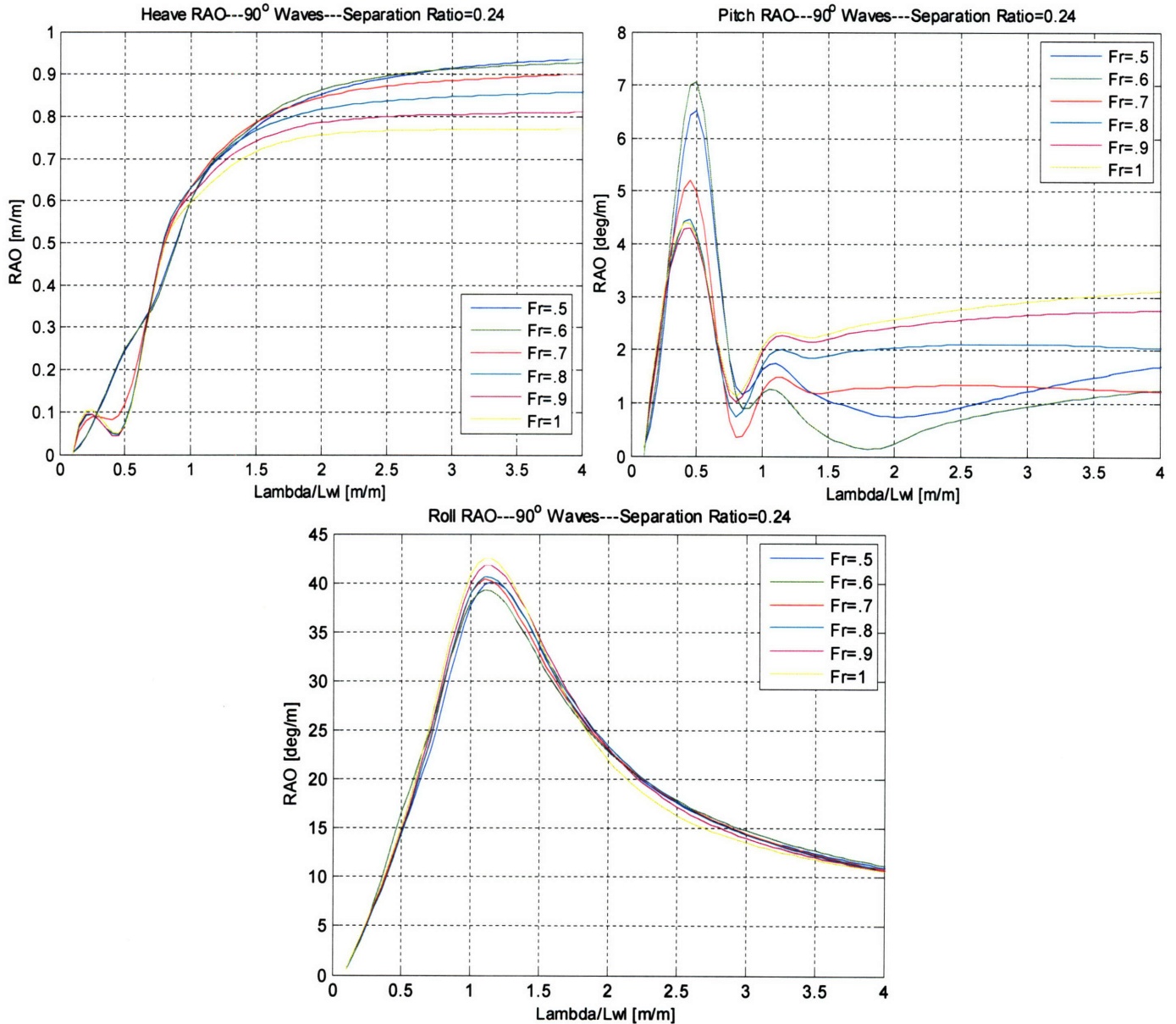


Figure 33 Pitch, Heave and Roll RAO in beam seas for each separation ratio

The dynamic trim correction provided by the control surface produced a single resonant response for each mode of motion and speed. Heave motion in particular appears

to be well damped and of little consequence over the entire Froude regime. Once again, the forward and aft hull geometric asymmetry generated a pitch response even in beam waves. Non-dimensional wavelengths producing significant response are extremely narrow banded and lie within the $\lambda / L_{Lwl} = .3$ to $.75$ range. The bow canards appear to limit pitch amplitude to less than $7^\circ/m$ making pitch in beam seas of little overall importance. Like the bare hull configuration however, roll RAO was of great importance. A well defined resonant non-dimensional wavelength of roughly 1.2 produced roll oscillations exceeding $40^\circ/m$. Recall bare hull peak roll RAO's were only slightly larger at $45^\circ/m$. Consequently, it appears bow mounted control surfaces produce only limited damping in roll. As previously stated, bow mounted foils are particularly suited to limiting vertical accelerations forward. Although roll motion does induce vertical motion, foils are mounted close to the roll center of rotation and therefore have a lower angular velocity than induced by pitch. This reduced velocity alters inflow angle only slightly therefore limiting damping force generated. Maximum RAO's are roughly constant over the entire speed regime. Although damping increases with forward speed, so do the roll excitation forces. These effects roughly cancel each other out to produce similar motion regardless of forward speed.

5.2.3 Port-Bow Seakeeping Response

The foil seakeeping response of each separation ratio in port-bow seas, or incident wave angle $\beta=135^\circ$, is presented below. Once again, the semi-SWATH was examined at six different forward speeds, from Froude number .5 to 1.0, with each mode of motion shown on a separate plot. Due to the semi-SWATH's port-starboard symmetry, the $\beta=135^\circ$ simulation is also a prediction of response in seas off the starboard bow.

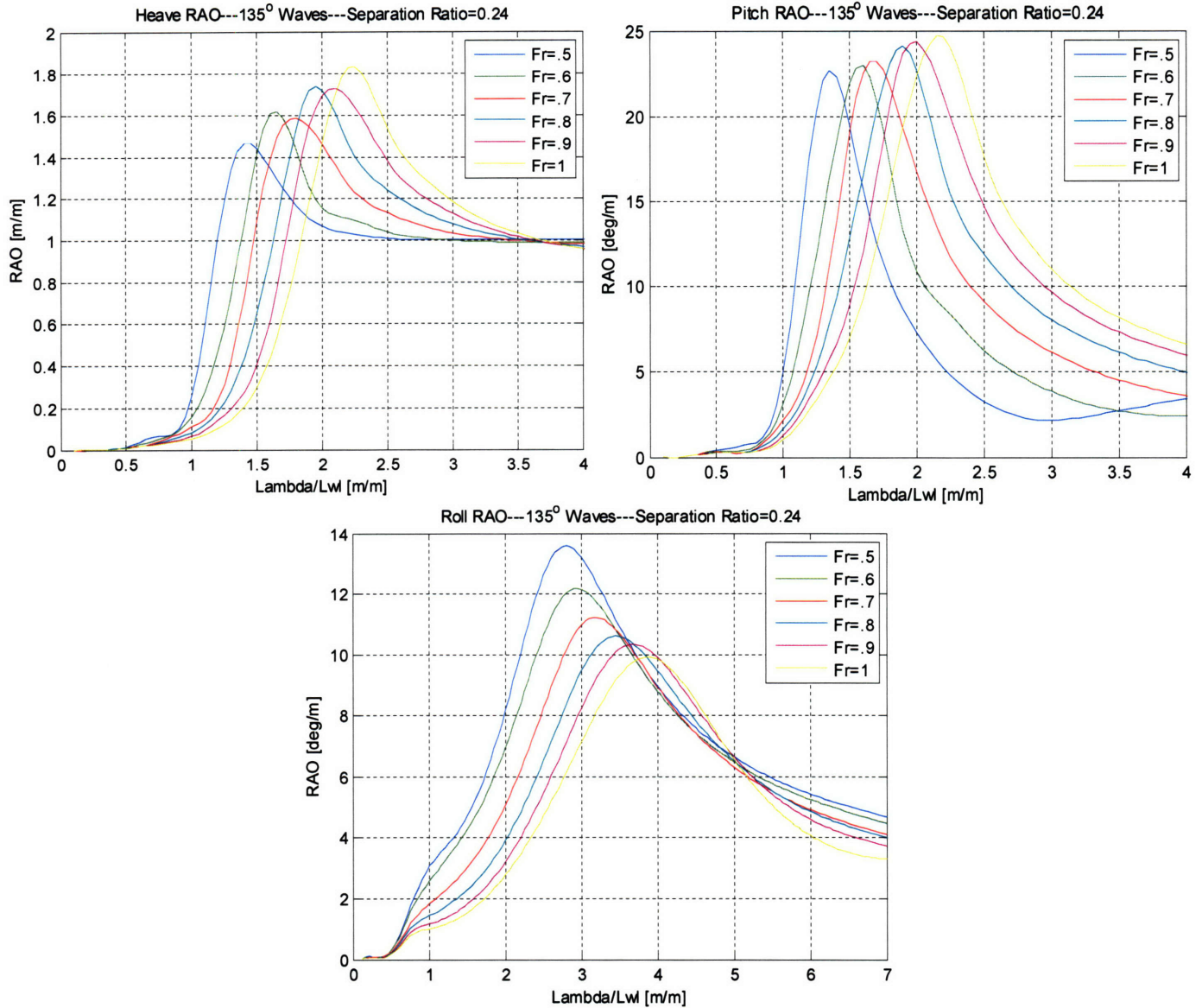


Figure 34 Heave, Pitch, and Roll RAO in port-bow seas for each separation ratio

Semi-SWATH motion in port-bow waves with bow foils shows a familiar single peaked resonant response. The foils' control of dynamic trim and passive damping eliminated the erratic bare hull response observed in identical ambient seas. The non-dimension wavelength exciting maximum heave and pitch response grew longer with forward speed and likely correspond to a single resonant encounter frequency. Both pitch perturbation and damping force increased with forward speed, however excitation force dominated total response at high-speed. It is interesting to note roll RAO exhibited the opposite behavior, suggesting damping effects dominate at high speeds.

5.3 Foil Controlled v. Bare Hull Seakeeping Response

The following figures present a comparison between the bare hull and foil controlled vessel response at the limits of the forward speeds studied in seakeeping, 10 and 20 knots. Because only the “as designed” demi-hull separation ratio, 0.24, was examined with foil control, the comparison below shows only bare hull results of the same separation.

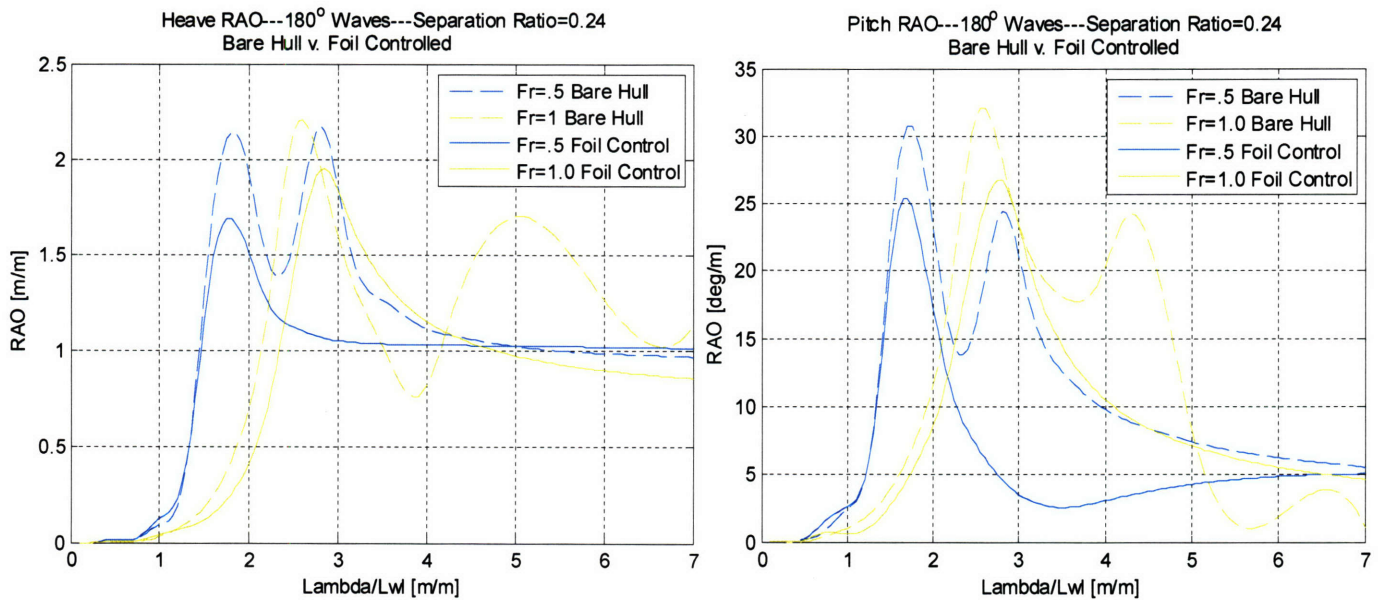


Figure 35 Heave & Pitch RAO of 0.24 separation ratio in head seas

A visual inspection of heave and pitch plots in Figure 35 reveals an approximate 25% reduction in peak oscillations when the quasi-active foil control system was in use. While the shorter wavelength bare hull maximum is closely mirrored by a foil damped peak, the longer wavelength one is absent in the foil response. The validity of this second peak is somewhat questionable, as wavelengths in excess of four boat lengths are not likely to produce significant motions. A mere reduction in second peak amplitude could be attributed to foil damping, but its complete absence suggests the second peak is due to excess steady trim angles exhibited by the uncontrolled bare hull. The figure below presents a heave, pitch, and roll comparison in beam seas. Heave, pitch and roll motions are presented in separate plots.

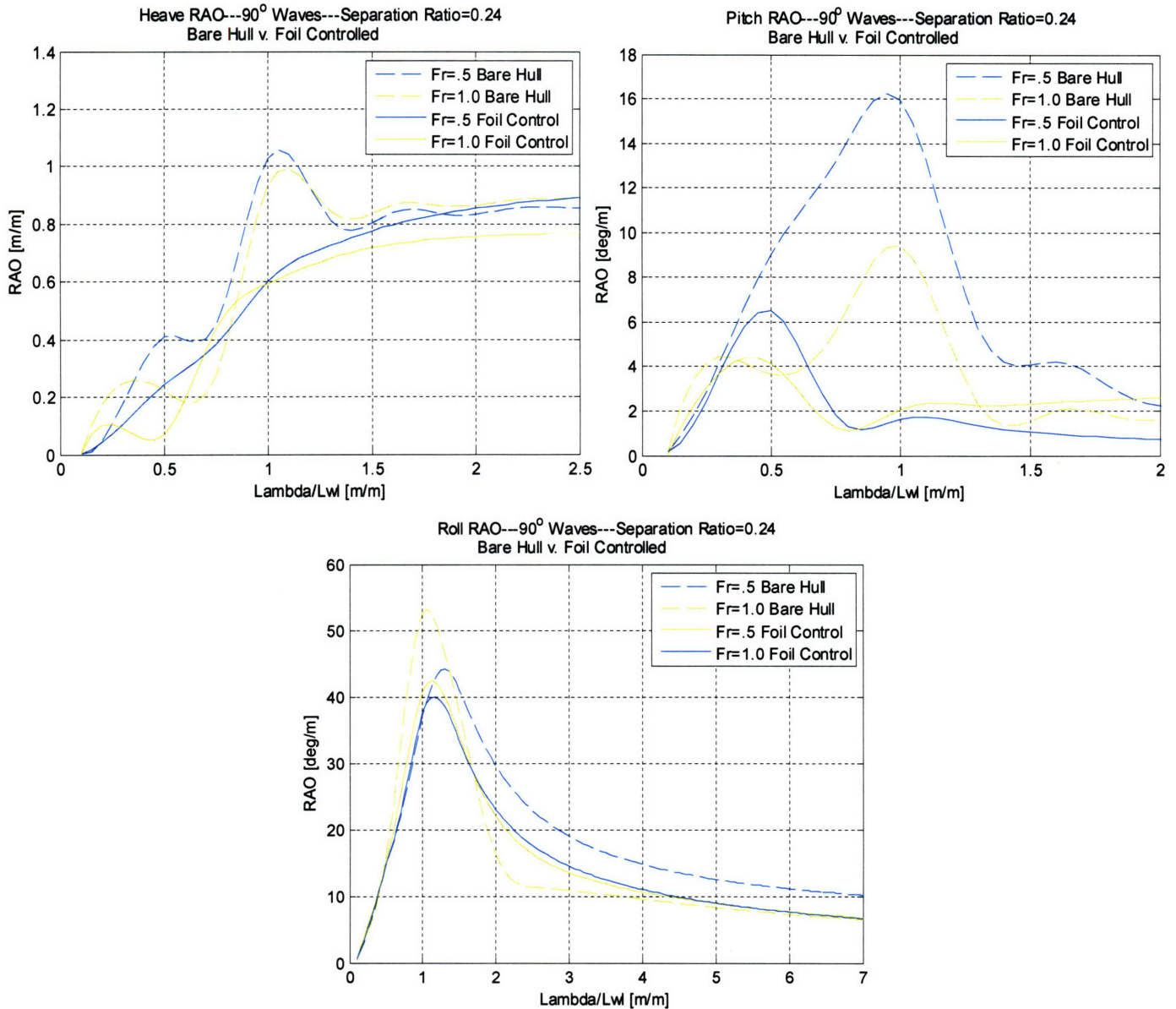


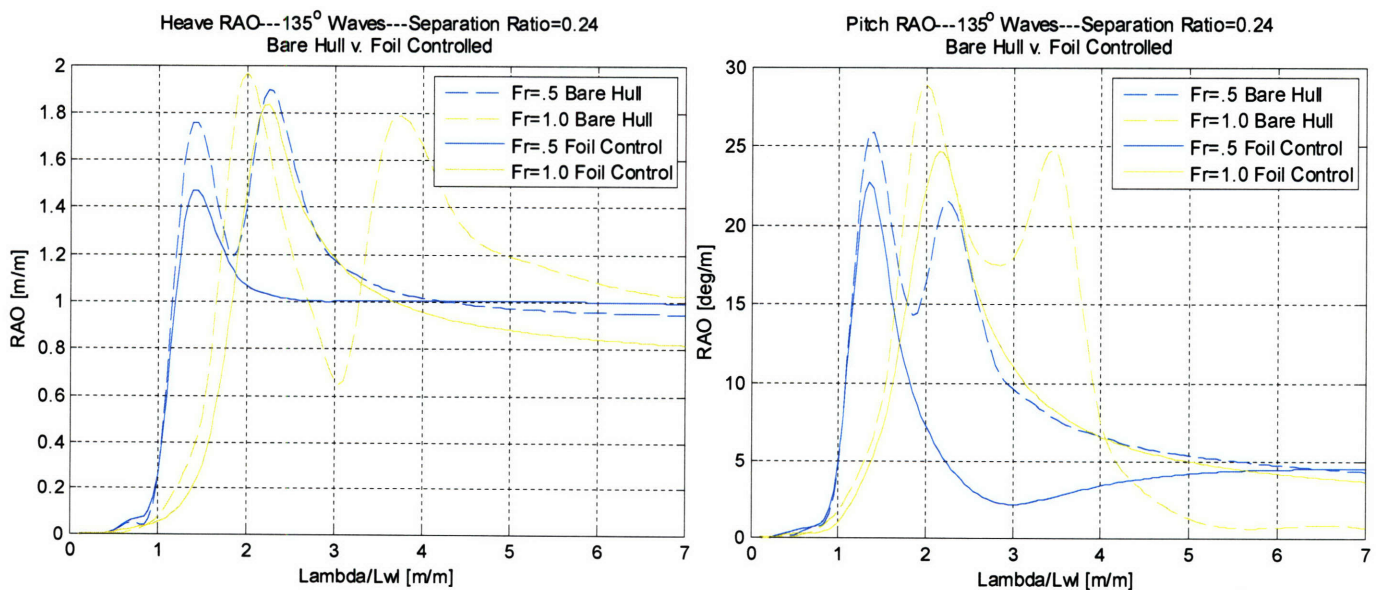
Figure 36 Heave, Pitch, and Roll RAO of 0.24 separation ratio in beam seas

Once again, the trim correction and additional damping provided by the control surfaces reduced oscillations in all modes of motion. The foil heave response smoothly approached unity at both forward speeds indicating foil damping has completely eliminated heave resonance in beam seas! Pitch motions were also dramatically reduced by a factor of two at both forward speeds. In addition to reducing the magnitude of the pitch response, the foil system significantly narrows the wavelength band that generates large motions. The bare hull is sensitive to non-dimensional wavelengths of .5 to 1.25, while significant foil response is limited to those within λ / L_{wl} of .4 to .6 . This sharpening of the response

peaks indicates superior seakeeping can be achieved through a small adjustment in encounter frequency. From an operational standpoint, this equates to a minor speed or course correction. Finally, a small reduction of 11% to 28% in roll RAO was observed with the foil controlled system. As expected, the magnitude of roll reduction is dependent on forward speed with higher Froude numbers producing more lift and hence damping force. As stated previously, the lower amount of appreciable damping in roll compared to pitch is attributed to the foils close proximity to the roll axis of the vessel.

Perhaps the most beneficial aspect of foil control is seen when considering pitch and roll motions simultaneously. As indicated by the dashed line in Figure 36, bare hull response peaks in pitch and roll occur at approximately the same resonant non-dimensional wavelength, $\lambda / L_{wl}=1$. In other words, a vessel operating at Froude number .5 in beam seas of 10.5m in wavelength would exhibit resonance in roll and pitch simultaneously! When using the quasi-active foil system, the resonant roll wavelength remained constant but the pitch wavelength was reduced by a factor of two. Because the pitch resonant peak is shifted to the left, the possibility of concurrent resonance in pitch and roll is completely eliminated.

Heave, pitch, and roll motions of the semi-SWATH were also examined in port-bow waves, $\beta=135^\circ$. The following figure presents a comparison of the vessel response in both control configurations.



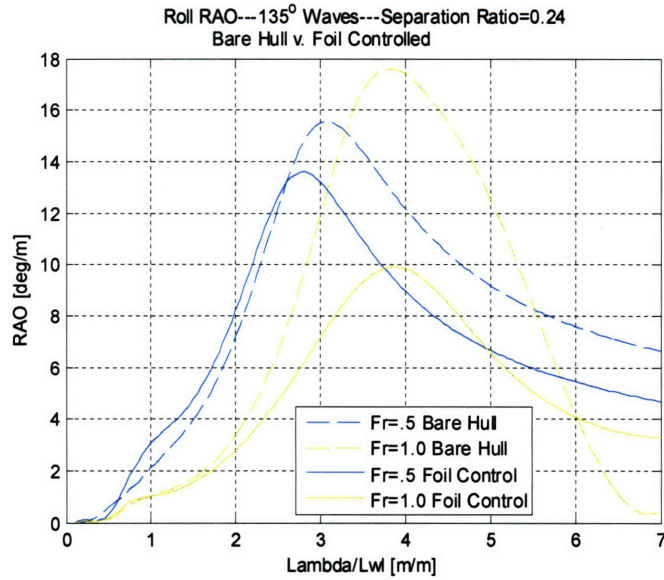


Figure 37 Heave, Pitch, and Roll RAO of 0.24 separation ratio in port-bow seas

Once again, foil damping and trim correction reduced the peak magnitude of oscillation in all modes of motion. A smaller range of waves produced resonant behavior when were foils in use. Beneficial motion damping increased with larger forward speeds further proving the system’s utility for use on high-speed vessels.

Chapter 6: Discussion and Conclusions

The hydrodynamic evaluation of a prototype 10,000kg reduced waterplane area twin hull was conducted in a numerical tow tank using the *SWAN2 2002* software package. The effect of demi-hull separation and quasi-active foil control on resistance and seakeeping was developed throughout the study. The following chapter provides a synopsis of results and recommendations for future work to be conducted.

6.1 Conclusions

Calm water simulations of each demi-hull separation were performed until forces and moments converged to produce a steady *Kelvin* wave pattern, sinkage, trim and ideal fluid resistance at forward speeds of 2 to 26 knots. Snapshots of wave patterns indicate transverse waves dominate at lower speeds, while divergent ones control the pattern above Froude number .6.

The anticipated high-speed dynamic vertical plane instability of the semi-SWATH was clearly shown in the sinkage and trim plots. Below Froude number .55, the bare hull vessel behaved very similarly to the conventional semi-displacement catamaran presented by the *Molland* study. At speeds above this critical Froude number, an increasing draft and bow down trim were observed. Attributable to an adverse pressure gradient near the bow, resulting trim angles exceeded those relevant for practical design purposes. This dramatic trim instability motivated the introduction of a quasi-active foil control system. The system was quasi-active in that the angle of attack of bow mounted canards was actuated based on the speed dependent trim moment needed to preserve design trim. Free surface foil interaction was explored with experimental data, and a conservative depth of 1.1m below the free surface was selected and held fixed for all subsequent foil simulations. Appendages were placed at the bow because previous studies have shown this location to be the optimal in reducing pitch and heave.

Foil controlled simulations were conducted over a speed range identical to the bare hull, and drag predictions included foil friction and induced drag. Enhancement of vessel performance was observed with foil control and through an increase in demi-hull separation. This was particularly true near the displacement hull “Froude Hump” of .55. The plots below review the need for, and the trim and resistance benefits of the foil canard system presented in Chapters 2 and 3.

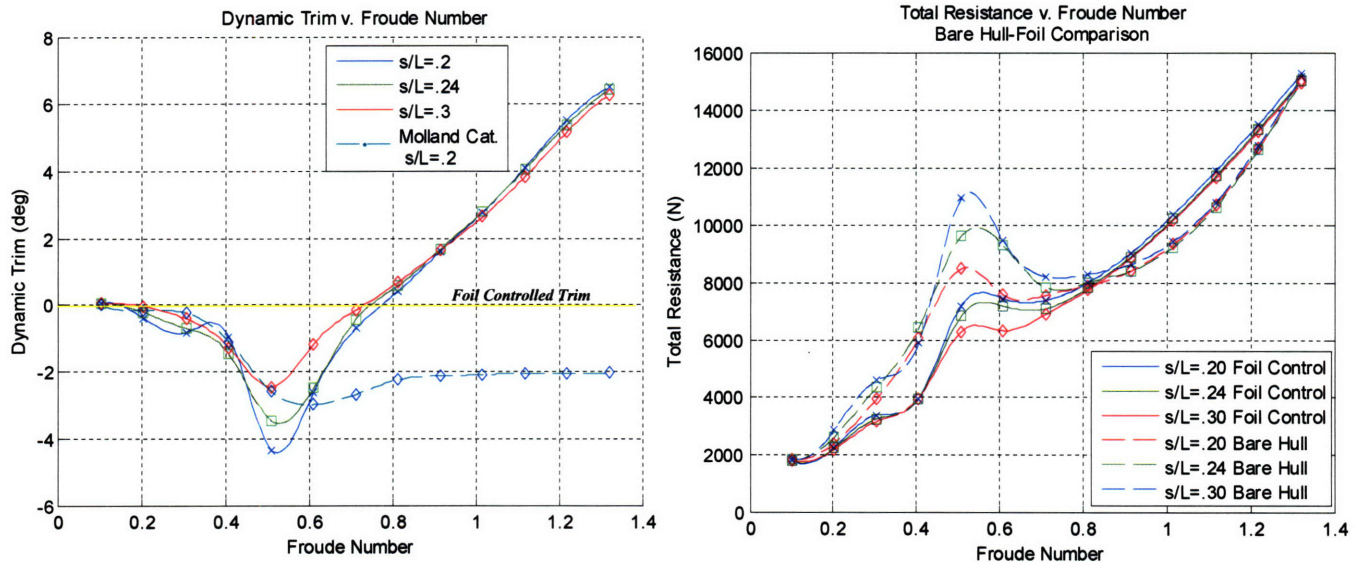


Figure 38 Review of dynamic trim and total resistance results

The bare hull seakeeping characteristics of each demi-hull separation were discussed in Chapter 4. The vessels were evaluated at forward speeds in the 10 to 20 knots range, operating in three different incident wave headings, $\beta = 90^\circ$, 135° , and 180° , as defined by *SWAN2* internal coordinate system. Several conclusions were gathered during the analysis of the hydrodynamic response. RAO plots revealed a high sensitivity to two particular wavelength creating dual resonant peaks. The first peak, induced by the lower wavelength, was approximately 1.75 times the length of the vessel in head wave and approximately half that in beam seas. The second peak often corresponded to wavelengths larger than three times the boat length and was an unexpected result. The excessive bow down trim angles might explain this behavior. The heave response of the semi-SWATH in bow waves revealed a single resonant wavelength. For all modes of motion and forward speeds, it is clear that increasing distance between the demi-hulls damps the response of the ratios studied.

The seakeeping response of the quasi-active foil control system was evaluated for the “as designed” demi-hull separation ratio of 0.24. The trim correction and passive damping afforded by the lifting foils suppressed heave and pitch motion amplitude by an impressive 20% to 50%. In all cases, the bare hull dual peak response was smoothed to a more conventional single peak. In the case of beam wave heave, both the peak amplitudes were damped out and the RAO smoothly approached unity. Foil control also reduced the beam seas resonant wavelength in roll by approximately half, thereby avoiding simultaneous occurrence of roll and pitch resonance as shown in the plot below.

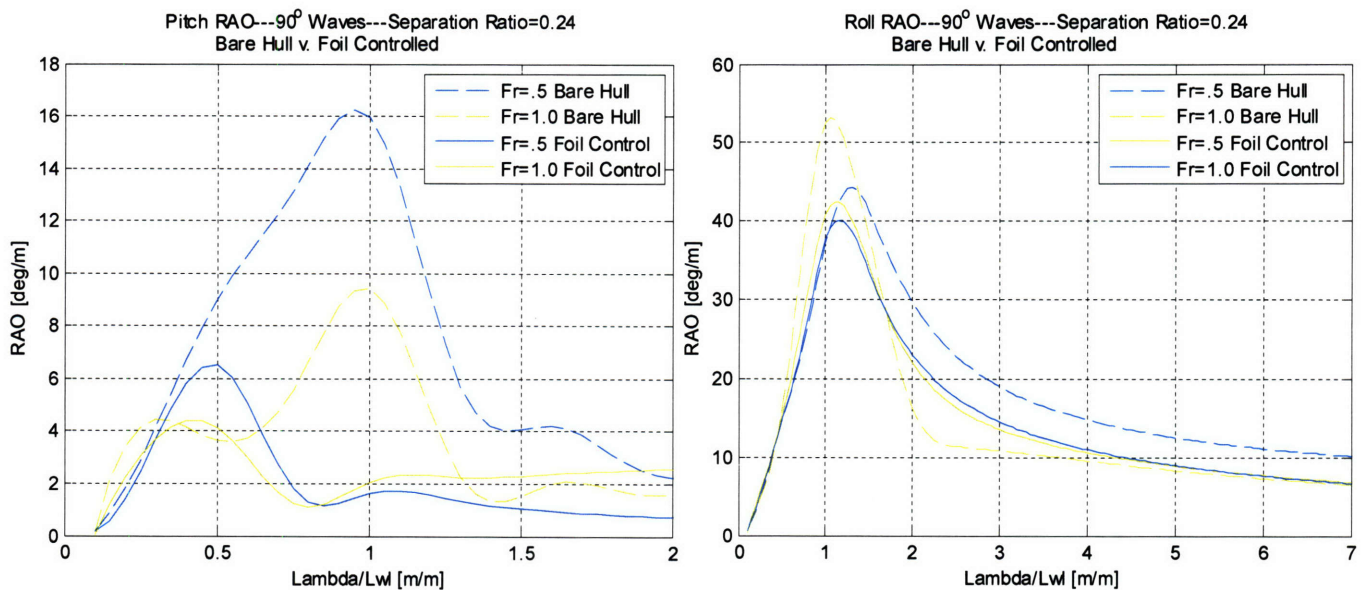


Figure 39 Avoiding simultaneous pitch and heave response through the use of quasi-active foil control

6.2 Recommendations For Future Work

Although *SWAN2 2002* is a validated state-of-the-art computational fluid dynamics code, the resistance and seakeeping results obtained for the semi-SWATH should be verified by tow tank testing. Resistance and seakeeping should be measured for an appropriately scaled ship model in calm water and waves generated by a wavemaker. The small relative size of the vessel examined, $L_{wl} = 10.5m$, lends itself well to this type of testing because scales up to one-half may be easily evaluated. The resulting data should be scaled and compared with those found in this paper. At the time of this printing, remarkably few model tests have been performed for exotic semi-displacement craft and in

particular reduced waterplane area twin hulls, making the validation of the current results of the utmost importance.

The evaluation of following seas and their impact on a semi-SWATH's behavior in a seaway was outside the scope of this paper. For a more complete picture of vessel performance, following waves should be analyzed. Added resistance, or the increase in resistance due to ambient waves, was also beyond the scope of this study and should be examined empirically or during tank testing. The resistance and seakeeping benefits of quasi-active foil control were thoroughly examined in this study. The next logical step is to introduce a fully active system capable of measuring accelerations and actuating foil angle to limit them. The *Laboratory for Ship and Platform Flows* is actively conducting applicable research on this topic.

Chapter 7: References

1. 'Principles of Naval Architecture', Volume III – "Motion in Waves and Controllability", Edward V. Lewis, 1989.
2. 'Sea Loads on Ships and Offshore Structures', O.M. Faltinsen, Cambridge Ocean Technology Series, 1990.
3. 'Hydrodynamics of High-Speed Marine Vehicles', Odd. M. Faltinsen, Cambridge University Press, 2005.
4. 'Hydrodynamic Design of High Speed Catamaran Vessels', S. Purvin, MIT Masters Thesis, 02/2003.
5. 'Marine Hydrodynamic', J.N. Newman, The MIT press, Cambridge Massachusetts, 1977.
6. 'Simulation Based Resistance and Seakeeping Performance of High-Speed Monohull and Multihull Vessels Equipped with Motion Control Lifting Appendages', P.D. Sclavounos, S. Purvin, T. Ulusoy, S. Kim, 'Fast 2003' Conference papers, Ischia, Italy, 2003.
7. 'Ocean Wave Interaction with Ships and Offshore Energy Systems', Sclavounos, P.D., Course 2.24 Class Notes, 2007, Massachusetts Institute of Technology.
8. 'SWAN-2 2002 Theory Manual', Boston Marine Consulting Inc.
9. 'SWAN-2 2002 User Manual', Boston Marine Consulting Inc.
10. 'Calm Water Powering Predictions for High-Speed Catamarans', P.R. Couser, A.F. Molland, N.A. Armstrong, I.K.A.P. Utama, 'Fast 97' conference papers, Sydney Australia, 1997.
11. 'Resistance Prediction for Fast Displacement Catamarans', S. Steen, H.J. Rambech, R. Zhao, K.J. Minsaas, 'FastShip' Conference papers, Washington, U.S.A, 1999.
12. 'Seakeeping Analysis for Preliminary Design', P. Couser, Formation Design Systems, 7/2000.

Appendix A: Semi-SWATH Principle Dimensions

The semi-SWATH analyzed in this study was provided by *Lockheed Martin Maritime Systems and Sensors* of Baltimore, MD. In accordance with a non-disclosure agreement, the hull offsets used in the hydrodynamic evaluation cannot be revealed. However, relevant principle vessel dimensions are presented below.

Principle Dimensions	
Length Overall	12m
Waterline Length	10.5m
Beam	3.2m
Displacement	10133kg
Draft	.75m
Longitudinal Center of Gravity	-0.26m
Vertical Center of Gravity	0.49m
Roll Radius of Gyration	1.57m
Pitch Radius of Gyration	2.83m
Yaw Radius of Gyration	2.89m

Table 1 Semi-SWATH principle dimensions. Amidships centered coordinate with positive x forward

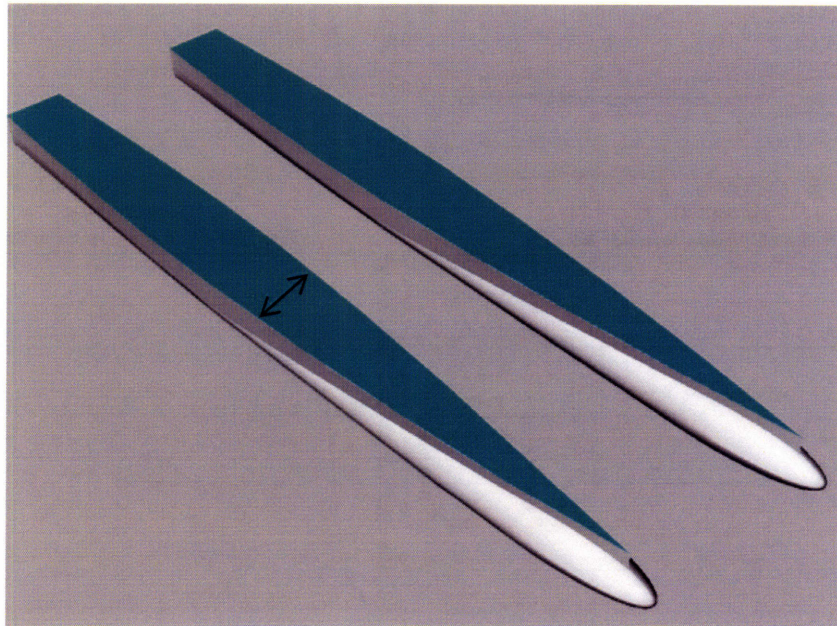
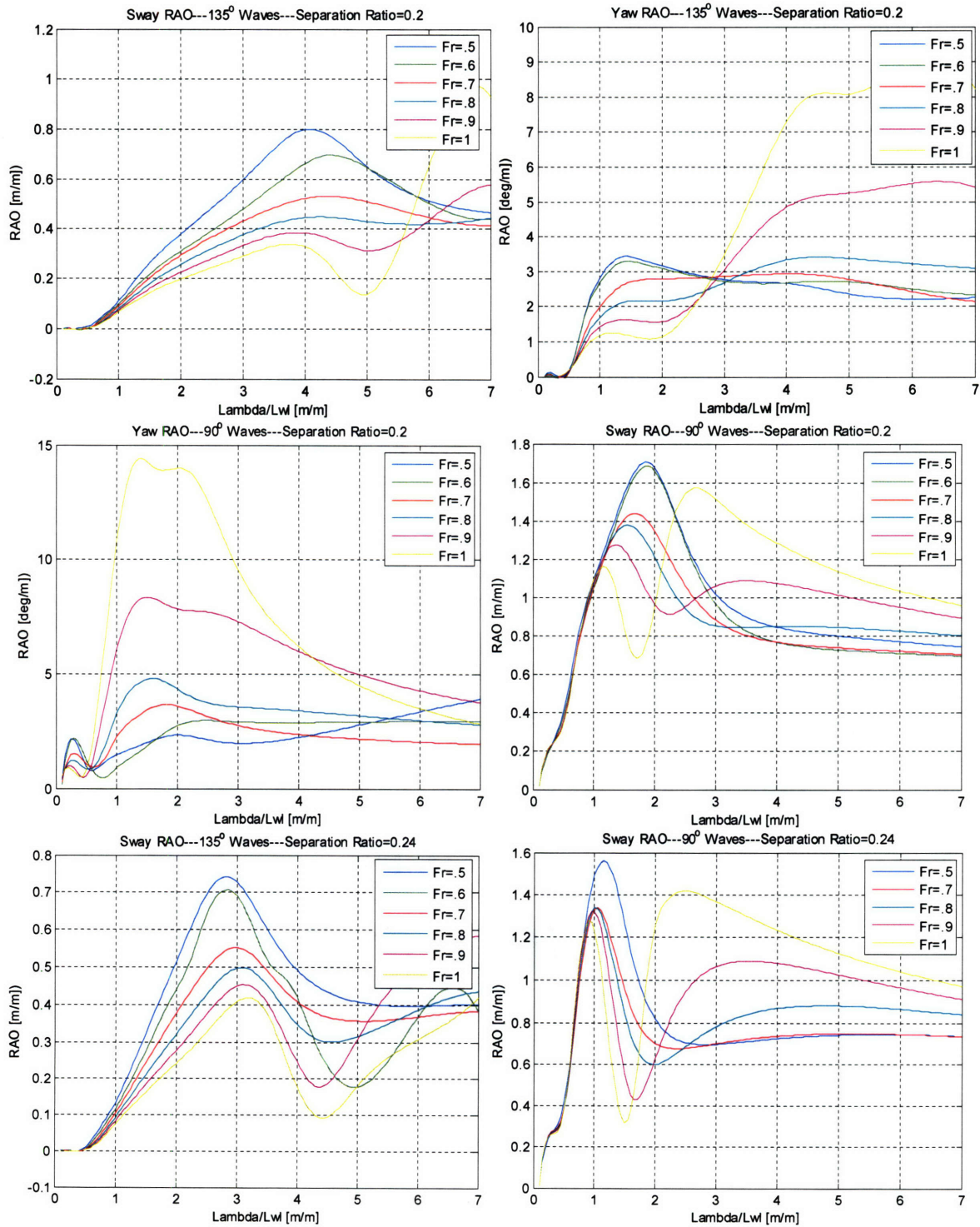
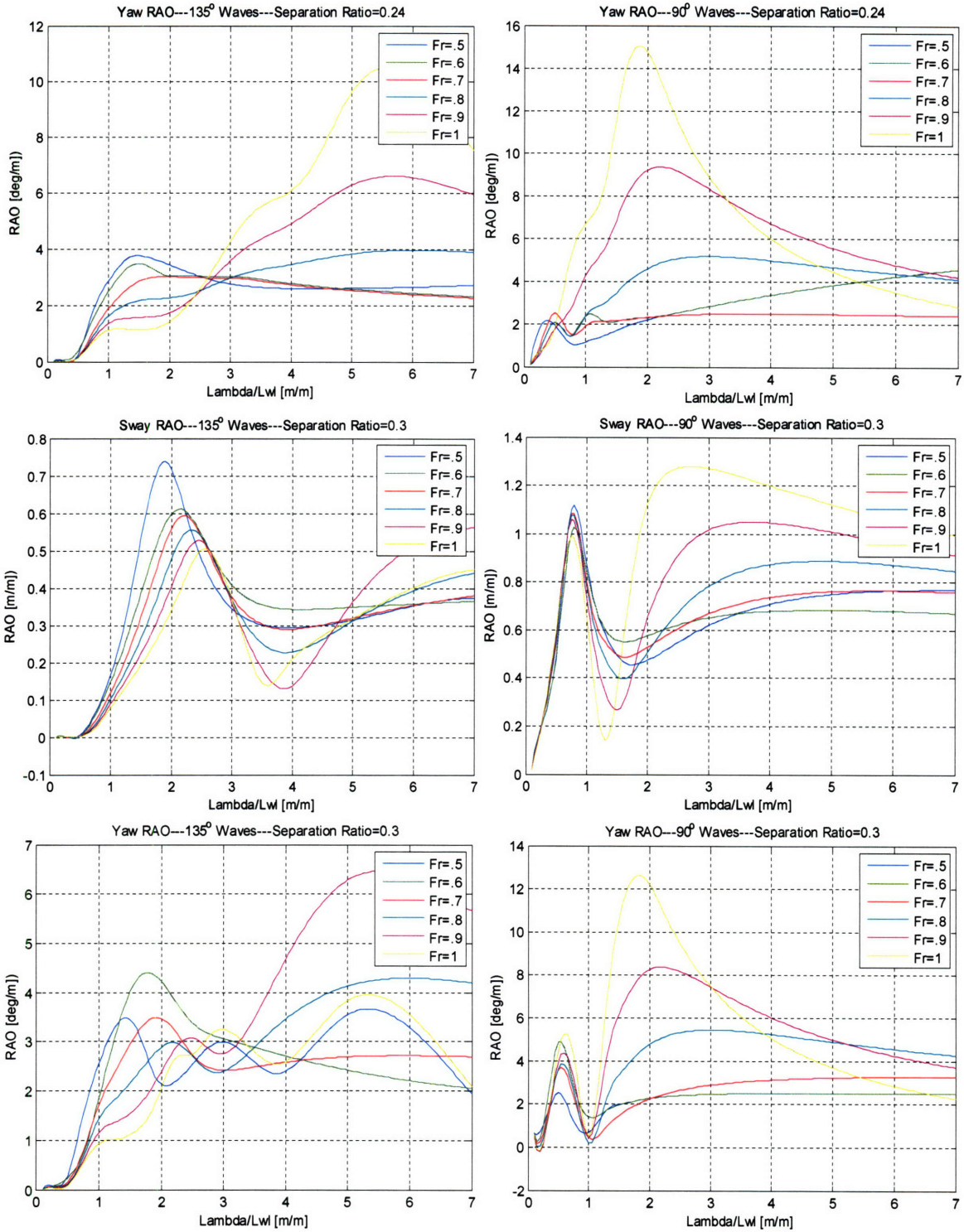


Figure 40 Semi-SWATH wetted surface. Note waterplane beam variation fore and aft

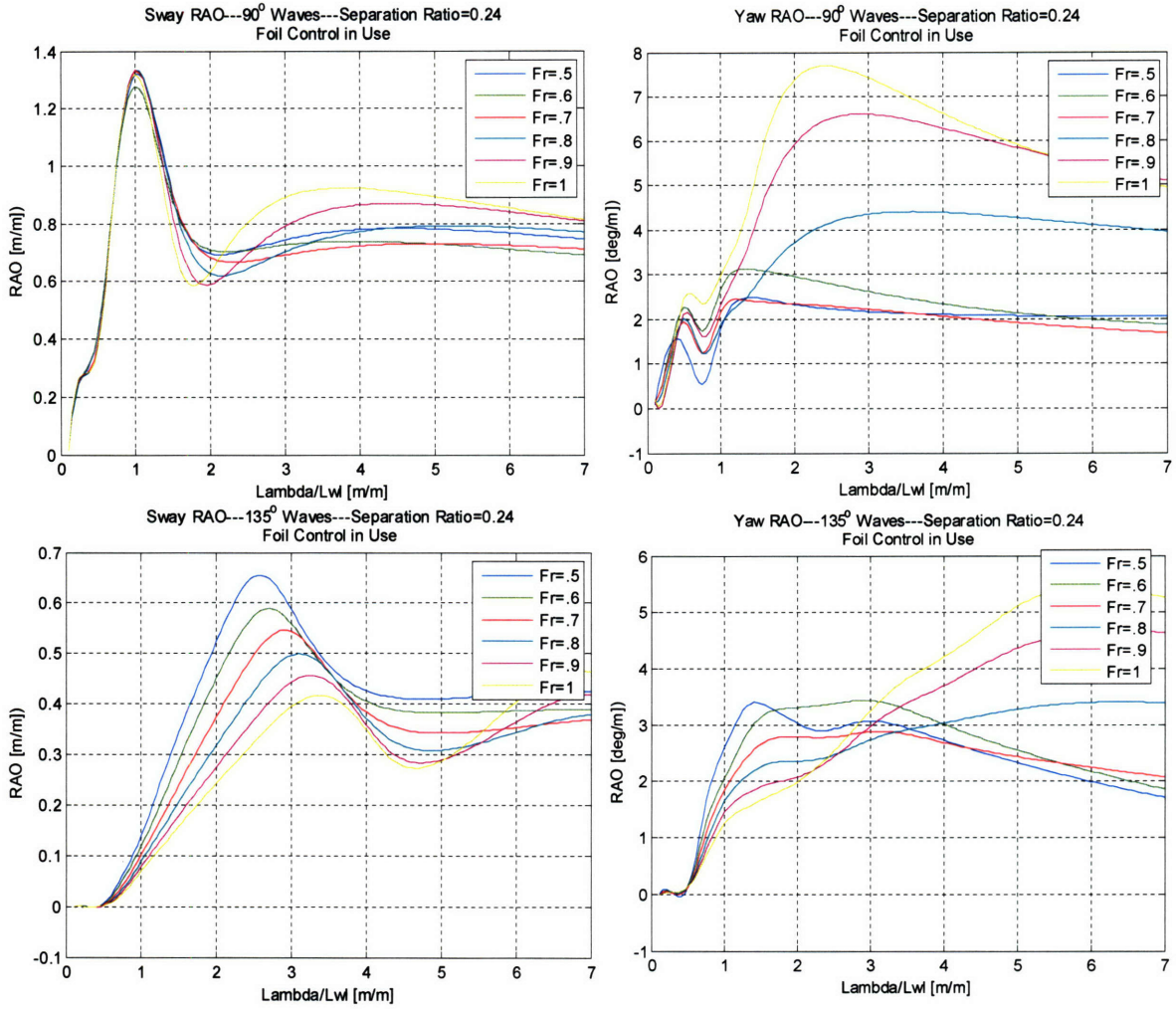
Appendix B: Sway and Yaw Response



Appendix B: Sway and Yaw Response



Appendix B: Sway and Yaw Response



Appendix C: Sample Sinkage & Trim Convergence Log

Hull Separation Ratio: 0.24 Ship Speed: 22 knots

It.#	Sinkage	Delta	Trim	Delta
1	3.003E-3	0.003003	2.826E+0	2.826000
2	-5.432E-2	0.057323	3.214E+0	0.388000
3	-6.963E-2	0.015310	3.676E+0	0.462000
4	-8.103E-2	0.011400	3.845E+0	0.169000
5	-8.625E-2	0.005220	3.961E+0	0.116000
6	-8.944E-2	0.003190	4.011E+0	0.050000
7	-9.076E-2	0.001320	4.044E+0	0.033000
8	-9.171E-2	0.000950	4.050E+0	0.006000
9	-9.168E-2	0.000030	4.073E+0	0.023000
10	-9.217E-2	0.000490	4.069E+0	0.004000

Time Completed: 3-15 00:57

Appendix D: Sample Seakeeping Response Log

*****Seakeeping Response*****

Hull Separation: 0.24 Heading: 135

Ship Speed: 10 knots

WL/Lwl	Surge	Sway	Heave	Roll	Pitch	Yaw	Ax	Ay	Az
--------	-------	------	-------	------	-------	-----	----	----	----

0.1	0.000	0.000	0.000	0.027	0.006	0.01	-0.26	0.27	-0.13
0.3	0.001	0.001	0.001	0.105	0.035	0.06	-0.39	0.37	-0.24
0.5	0.006	0.006	0.015	0.321	0.409	0.14	-1.01	0.13	-0.94
0.8	0.024	0.061	0.067	1.797	0.770	1.67	-1.45	-0.44	-2.18
1.0	0.128	0.139	0.258	3.076	4.949	2.61	-5.48	-1.25	-5.50
1.3	0.402	0.264	1.337	3.979	22.098	3.34	-14.23	-2.32	-19.42
1.6	0.185	0.381	1.348	5.259	15.702	3.32	-6.43	-2.62	-14.55
1.9	0.034	0.489	1.107	7.340	8.650	3.09	-2.21	-2.52	-9.39
2.2	0.057	0.591	1.035	10.076	5.237	2.92	-1.34	-2.26	-7.16
2.5	0.112	0.653	1.011	12.644	3.274	2.93	-1.15	-1.87	-5.87
2.8	0.156	0.634	1.003	13.595	2.315	3.04	-1.08	-1.38	-5.00
3.1	0.194	0.562	1.003	12.805	2.233	3.06	-1.10	-0.99	-4.35
3.5	0.239	0.477	1.004	10.924	2.740	2.95	-1.15	-0.71	-3.71
3.9	0.279	0.433	1.006	9.296	3.291	2.77	-1.17	-0.61	-3.22
4.3	0.316	0.415	1.007	8.084	3.720	2.60	-1.17	-0.57	-2.84
5.0	0.372	0.411	1.006	6.657	4.194	2.33	-1.12	-0.55	-2.33
6.0	0.431	0.420	1.002	5.439	4.471	2.00	-1.01	-0.51	-1.84
7.0	0.465	0.425	0.996	4.675	4.502	1.72	-0.88	-0.46	-1.51

Ship Speed: 12 knots

Λ/Lwl	Surge	Sway	Heave	Roll	Pitch	Yaw	Ax	Ay	Az
-------	-------	------	-------	------	-------	-----	----	----	----

0.1	0.000	0.000	0.000	0.027	0.005	0.01	-0.26	0.41	-0.13
0.3	0.001	0.001	0.001	0.102	0.035	0.05	-0.49	0.47	-0.32
0.5	0.005	0.004	0.014	0.340	0.354	0.16	-1.09	0.36	-1.04
0.8	0.016	0.052	0.052	1.597	0.483	1.30	-1.13	-0.40	-2.05
1.0	0.088	0.119	0.160	2.604	3.116	2.06	-4.34	-1.30	-4.08
1.3	0.286	0.218	0.740	3.585	14.087	2.84	-11.27	-2.14	-12.72
1.6	0.350	0.323	1.608	4.715	22.982	3.23	-12.05	-2.52	-20.37
1.9	0.134	0.421	1.259	6.334	13.315	3.30	-4.76	-2.51	-12.43
2.2	0.041	0.510	1.105	8.445	8.746	3.33	-2.16	-2.31	-8.84

Appendix D: Sample Seakeeping Response Log

2.5	0.047	0.575	1.040	10.644	6.237	3.38	-1.41	-1.98	-6.95
2.8	0.089	0.586	1.010	12.027	4.622	3.43	-1.20	-1.54	-5.76
3.1	0.126	0.540	0.997	11.988	3.539	3.42	-1.08	-1.12	-4.94
3.5	0.170	0.462	0.991	10.626	2.713	3.27	-1.01	-0.77	-4.15
3.9	0.209	0.413	0.992	9.120	2.422	3.06	-0.98	-0.63	-3.59
4.3	0.244	0.391	0.993	7.920	2.443	2.86	-0.98	-0.58	-3.15
5.0	0.298	0.383	0.995	6.481	2.703	2.55	-0.96	-0.55	-2.58
6.0	0.359	0.387	0.993	5.252	3.003	2.18	-0.89	-0.51	-2.02
7.0	0.399	0.390	0.988	4.480	3.138	1.86	-0.80	-0.46	-1.65

Ship Speed: 14 knots

Λ/Lwl Surge Sway Heave Roll Pitch Yaw Ax Ay Az

0.1	0.000	0.000	0.000	0.022	0.004	0.00	-0.32	0.38	-0.18
0.3	0.001	0.000	0.001	0.074	0.027	0.04	-0.47	0.44	-0.32
0.5	0.005	0.003	0.012	0.281	0.332	0.13	-1.27	0.42	-1.07
0.8	0.010	0.041	0.041	1.205	0.364	1.10	-0.93	-0.46	-1.96
1.0	0.066	0.102	0.111	1.841	2.173	1.85	-3.71	-1.61	-3.34
1.3	0.196	0.183	0.426	2.515	8.928	2.43	-8.63	-2.35	-8.57
1.6	0.396	0.268	1.395	3.389	22.564	2.73	-14.48	-2.63	-20.49
1.9	0.264	0.349	1.547	4.615	19.326	2.79	-8.75	-2.60	-17.59
2.2	0.121	0.427	1.269	6.269	12.575	2.78	-4.13	-2.41	-11.64
2.5	0.055	0.498	1.134	8.273	9.129	2.79	-2.23	-2.14	-8.64
2.8	0.045	0.543	1.065	10.181	7.098	2.85	-1.50	-1.79	-6.89
3.1	0.071	0.536	1.027	11.181	5.746	2.89	-1.24	-1.36	-5.75
3.5	0.110	0.465	1.000	10.683	4.539	2.84	-1.08	-0.88	-4.72
3.9	0.146	0.397	0.986	9.294	3.757	2.72	-0.99	-0.62	-4.00
4.3	0.180	0.359	0.978	7.977	3.237	2.60	-0.94	-0.53	-3.47
5.0	0.233	0.343	0.970	6.320	2.685	2.44	-0.87	-0.51	-2.79
6.0	0.298	0.354	0.963	4.931	2.286	2.25	-0.81	-0.51	-2.17
7.0	0.348	0.369	0.958	4.115	2.092	2.08	-0.74	-0.48	-1.76

Ship Speed: 16 knots

Λ/Lwl Surge Sway Heave Roll Pitch Yaw Ax Ay Az

0.1	0.000	0.000	0.000	0.020	0.004	0.00	-0.36	0.43	-0.20
0.3	0.001	0.000	0.001	0.065	0.024	0.03	-0.50	0.47	-0.36
0.5	0.005	0.002	0.011	0.244	0.297	0.14	-1.37	0.47	-1.16
0.8	0.007	0.034	0.036	1.042	0.343	0.92	-0.90	-0.37	-2.00
1.0	0.053	0.089	0.085	1.453	1.658	1.66	-3.37	-1.80	-2.98
1.3	0.148	0.159	0.284	1.910	6.497	2.10	-7.40	-2.53	-6.60
1.6	0.314	0.230	0.928	2.563	16.579	2.31	-12.61	-2.74	-15.65

Appendix D: Sample Seakeeping Response Log

1.9	0.381	0.297	1.719	3.534	24.120	2.35	-13.14	-2.66	-22.31
2.2	0.213	0.363	1.465	4.875	16.712	2.38	-6.78	-2.45	-15.25
2.5	0.118	0.426	1.244	6.558	11.897	2.48	-3.69	-2.19	-10.71
2.8	0.072	0.478	1.128	8.392	9.252	2.63	-2.29	-1.88	-8.22
3.1	0.062	0.500	1.060	9.921	7.596	2.79	-1.64	-1.51	-6.66
3.5	0.082	0.464	1.007	10.597	6.148	2.92	-1.28	-0.98	-5.31
3.9	0.111	0.389	0.976	9.786	5.185	3.01	-1.12	-0.60	-4.41
4.3	0.141	0.332	0.956	8.476	4.504	3.11	-1.02	-0.43	-3.76
5.0	0.193	0.309	0.934	6.518	3.682	3.28	-0.92	-0.44	-2.98
6.0	0.261	0.344	0.916	4.864	2.914	3.40	-0.83	-0.54	-2.27
7.0	0.319	0.380	0.906	3.996	2.387	3.39	-0.77	-0.55	-1.82

Ship Speed: 18 knots

Δ/Lwl	Surge	Sway	Heave	Roll	Pitch	Yaw	Ax	Ay	Az
--------------	-------	------	-------	------	-------	-----	----	----	----

0.1	0.000	0.000	0.000	0.018	0.004	0.00	-0.41	0.48	-0.20
0.3	0.001	0.000	0.001	0.057	0.021	0.03	-0.53	0.50	-0.39
0.5	0.005	0.002	0.010	0.207	0.280	0.14	-1.54	0.44	-1.22
0.8	0.005	0.029	0.032	0.908	0.308	0.80	-0.84	-0.32	-2.08
1.0	0.042	0.079	0.067	1.180	1.284	1.45	-3.07	-1.95	-2.69
1.3	0.117	0.139	0.200	1.512	4.981	1.78	-6.58	-2.65	-5.31
1.6	0.241	0.200	0.624	2.054	12.112	1.95	-10.71	-2.80	-11.97
1.9	0.408	0.257	1.549	2.898	23.679	2.04	-15.10	-2.67	-22.75
2.2	0.313	0.314	1.687	4.057	21.167	2.19	-10.18	-2.43	-19.80
2.5	0.184	0.369	1.382	5.510	14.726	2.44	-5.51	-2.17	-13.37
2.8	0.120	0.419	1.203	7.162	11.167	2.77	-3.36	-1.89	-9.82
3.1	0.090	0.452	1.100	8.781	9.071	3.08	-2.30	-1.56	-7.72
3.5	0.086	0.445	1.019	10.195	7.330	3.39	-1.63	-1.04	-5.98
3.9	0.102	0.379	0.971	10.133	6.205	3.63	-1.33	-0.57	-4.86
4.3	0.126	0.309	0.939	8.991	5.429	3.91	-1.17	-0.32	-4.09
5.0	0.173	0.290	0.904	6.652	4.530	4.36	-1.02	-0.41	-3.17
6.0	0.240	0.365	0.874	4.611	3.730	4.66	-0.92	-0.66	-2.37
7.0	0.302	0.420	0.856	3.734	3.205	4.63	-0.84	-0.71	-1.87

Ship Speed: 20 knots

Δ/Lwl	Surge	Sway	Heave	Roll	Pitch	Yaw	Ax	Ay	Az
--------------	-------	------	-------	------	-------	-----	----	----	----

0.1	0.000	0.000	0.000	0.017	0.002	0.00	-0.32	0.54	-0.34
0.3	0.001	0.000	0.001	0.051	0.020	0.03	-0.59	0.54	-0.38
0.5	0.005	0.002	0.009	0.178	0.267	0.14	-1.72	0.41	-1.27
0.8	0.003	0.025	0.029	0.803	0.283	0.69	-0.77	-0.28	-2.14
1.0	0.034	0.070	0.053	1.006	1.015	1.26	-2.81	-2.02	-2.45

Appendix D: Sample Seakeeping Response Log

1.3	0.095	0.123	0.146	1.264	3.984	1.54	-6.03	-2.72	-4.41
1.6	0.192	0.176	0.443	1.742	9.283	1.73	-9.41	-2.82	-9.60
1.9	0.354	0.227	1.182	2.493	19.374	1.92	-14.21	-2.67	-19.51
2.2	0.399	0.276	1.831	3.500	24.634	2.18	-13.71	-2.43	-24.05
2.5	0.253	0.325	1.540	4.741	17.648	2.55	-7.71	-2.17	-16.62
2.8	0.166	0.370	1.289	6.169	12.927	2.97	-4.58	-1.89	-11.70
3.1	0.123	0.405	1.145	7.662	10.264	3.39	-3.04	-1.59	-8.91
3.5	0.103	0.415	1.035	9.322	8.165	3.83	-2.05	-1.11	-6.71
3.9	0.107	0.368	0.970	9.907	6.862	4.13	-1.59	-0.60	-5.36
4.3	0.124	0.296	0.928	9.172	5.987	4.46	-1.34	-0.27	-4.44
5.0	0.164	0.288	0.883	6.573	5.016	5.11	-1.13	-0.45	-3.39
6.0	0.228	0.404	0.843	4.068	4.202	5.46	-1.00	-0.88	-2.49
7.0	0.290	0.464	0.819	3.289	3.700	5.25	-0.92	-0.90	-1.95

Time Completed: 4-15 13:22